Factors Influencing the Design and Performance of Mars Entry Vehicles

P. LEVINE, T. R. ELLIS, AND S. GEORGIEV
Avco Corporation, Wilmington, Mass.

Nomenclature

A = reference area
B = planetary miss distance, $r_p\,(1 + 2\mu/r_pV_\infty^2)^{1/2}$, in Fig. 2, ft (or km)
B_r = receiver bandwidth [Eq. (1) and Fig. 4], cps
C_D = drag coefficient
$C_{L\alpha}$ = lift curve slope
$(C_{m_q} + C_{m_{\dot\alpha}})$ = pitch damping coefficient
D = diameter, ft
F = receiver noise figure [Eq. (1)]
f = frequency, cps
G = total antenna gain
g = gravitational acceleration; g_c at Mars surface = 12.3 ft/sec^2
h_{scale} = atmosphere scale height, ft (or km)
K_n = noise power density, w-sec/cycle
L_a = atmospheric losses (Earth + Mars, if direct link)
L_c = total circuit loss
L_s = free space loss
l = reference length, ft
$\mathfrak{M}$ = molecular weight
m = mass, slug
P_t = transmitted power, w
p = pressure; p_{surf} = surface pressure on Mars, psf (or mb, if stated)
p_s = stagnation pressure, psf
Q = integrated heat load during entry, Btu/ft^2
$\dot Q$ = heat flux; $\dot Q_c$ = convective flux at stagnation point; $\dot Q_r$ = radiative flux, Btu/ft^2-sec
q = dynamic pressure = $\rho V^2/2$, psf
R = slant range, ft (or km)
Re = local Reynolds number
R_N = nose radius, ft
R_{snt} = threshold signal/noise ratio
r_p = periapsis radius, ft (or km)
S = surface area; S_N refers to nose, or high heat load region; S_{AB} refers to afterbody or low heat load region, ft^2
V = velocity, fps
W = weight
X = mole fraction in Mars atmosphere (e.g., X_{CO_2} is mole fraction of carbon dioxide)
$X_{c.g.}$ = location of center of gravity, measured from nose, ft
$X_{c.p.}$ = location of center of pressure, measured from nose, ft
α = angle of attack, deg (or rad)
β = inverse of scale height, h_{scale}^{-1}, ft^{-1} (or km^{-1})
γ = flight path angle; positive in climb, deg
μ = gravitational product of attracting planet, ft^3/sec^2 (or km^3/sec^2)
ρ = density
σ = radius of gyration; also standard deviation

Subscripts

e = condition at entry into Mars atmosphere
HS = heat shield plus structure
S = suspended (by main chute)
∞ = freestream conditions

Mr. Philip Levine is Senior Staff Engineer in the Space Systems Directorate in the Avco Research and Advanced Development Division (RAD). He has served as project leader on research contracts on planetary entry vehicle concepts, including configuration, aerothermodynamic, and structural aspects since 1961. Mr. Levine received the M. S. degree in Aeronautical Engineering from Ohio State University in 1956. Prior to joining Avco in 1956, Mr. Levine was a Task Scientist at the Aeronautical Research Laboratory at Wright Field and an Aeronautical Research Scientist at NASA Langley. He has taught courses on aerospace vehicle design and has numerous publications on ballistic and lifting entry vehicle design. He is a member of AIAA.

Mr. T. R. Ellis is Manager, System Design in the Space Systems Directorate of Avco/RAD. He has been responsible for the system engineering efforts on a number of planetary mission programs. Prior to this assignment he directed over-all instrumentation design efforts on several ICBM re-entry vehicle programs. Mr. Ellis received the M. S. degree in Physics and Mathematics from Northeastern University in 1961. Prior to joining Avco, Mr. Ellis was a member of the Bell Telephone Laboratories Technical Staff. He is a member of AIAA.

Mr. S. Georgiev is Manager, Advanced Projects in the Space Systems Directorate of Avco/RAD. He has contributed to the current planetary entry programs at Avco as well as a number of military space programs. Prior to this assignment he directed the aerophysics activities for the division. Mr. Georgiev received the B.S. Engineering Physics degree from Cornell University in 1957. Prior to joining Avco/RAD in 1961 he was a member of the Senior Staff at the Avco-Everett Research Laboratory where he was engaged in research on hypersonic heat transfer, ablation, and radiative heating phenomena. He is a member of AIAA.

Presented as Preprint 63-476 at the AIAA/CASI/RAeS 9th Anglo-American Conference, Cambridge, Mass., October 16–18, 1963, and Montreal, Canada, October 21–24, 1963; revision received December 31, 1964; Published with the permission of The Royal Aeronautical Society and the Canadian Aeronautics and Space Institute. The results presented herein have been obtained partially under NASA Contracts NASw 697, JPL 950626, and JPL 950986. The authors wish to acknowledge the valuable contributions of many members of the technical staff at the Avco Research and Advanced Development Division, specifically, M. D. Russell, G. J. Cloutier, P. C. DiCarlo, and A. Robb in connection with entry vehicle design considerations; R. Barnes, D. Fields, J. J. Hayes, and M. Koslover in connection with the over-all mission considerations; and E. Botan in connection with the sterilization considerations.

Introduction

SPECULATION on the presence and extent of life on Mars has long held the interest of the scientific community. To determine the presence and the characteristics of life on Mars, it is desirable to place substantial scientific payloads on the planetary surface and to perform biological experiments over a period spanning seasonal variations. This paper reviews some of the recent progress on Mars entry vehicle design concepts and illustrates the relative importance of mission objectives, launch and trajectory constraints, uncertainties in the planetary atmospheric characteristics, sterilization requirements, and communications requirements on the performance of unmanned entry vehicles. (The entry vehicles are assumed to be transported to the vicinity of Mars by a "bus" spacecraft, but the questions of bus design are not treated here. It is realized, however, that the bus and lander designs are usually heavily interrelated and must be jointly considered for each interplanetary mission.) For convenience, the paper has been divided into three main parts: a description of some of the more important over-all mission requirements, a discussion of the problem of entry into Mars and payload protection on landing, and a review of some typical design concepts for each mission category.

General Mission Requirements

Early Missions

The problems of design and development of spacecraft and entry vehicles to search for extraterrestrial life on Mars are complicated by the fact that we possess only fragmentary knowledge of the atmospheric and surface characteristics of the planet. (The scientific objectives and experimental design could lead to the selection of most desirable landing sites[1] on Mars.) The large uncertainties in these characteristics lead to conservative lander vehicle design criteria.

Most of the early Mars entry missions can be grouped into three broad categories: 1) atmospheric probes, 2) short-lifetime landers, and 3) long-lifetime landers. Atmospheric probes obtain data on ambient pressure, density, scale height, temperature, and atmospheric composition; since they are not required to survive impact, they could weigh as little as 20 lb. They could include diagnostic instrumentation to determine the entry vehicle performance. Short-lifetime landers to perform limited experiments over a period of a few hours or days could be designed for about 500 lb and thus might be compatible with injected-weight capabilities of early launch vehicles. (In addition to the lander vehicle itself, the mission must provide for the flyby bus and the separation system between bus and the lander; thus, the total injected weight for the early missions could be $\sim$1500 lb.) In addition to atmospheric measurements during entry, they could also perform a few measurements and/or simple experiments on the ground. For example, a single simple biological experiment plus a measurement of the surface wind velocity might comprise the total landed experimentation for the early vehicles. The later, long-lifetime landers could weigh in excess of 4000 lb (and as high as 25,000 lb), and, in addition to biological experiments, they could carry instruments for atmospheric analysis by infrared and ultraviolet absorption and emission spectroscopy, television cameras, seismic instruments, and a core drill and mill. The following sections present important factors that should be considered in the synthesis of a vehicle design for a given mission.

Sterilization of Entry and/or Lander Vehicles

Sterilization is necessary to protect Mars from contamination by Earth organisms that might alter its ecology and interfere with subsequent attempts at biological observation.[2-4] Sterilization standards have been established based upon the probabilities of contaminating the planet assuming two launches to Mars for every launch opportunity by both the United States and Soviet Russia. It is argued that the risk of contaminating the planet should be smaller than the probability of obtaining no useful biological data for all other reasons: this results in a requirement that for each launch the probability of contaminating Mars with viable terrestrial organisms be less than 10^{-4}.[5] One solution is to avoid any contact between the spacecraft and the planet or its atmosphere. This approach is acceptable only for high-altitude orbiters (or flyby vehicles), which accordingly must have a minimum orbital altitude of approximately 4000 km for nearly circular orbits in order to prevent decay of the trajectory to a dangerous degree for at least 50 yr. For entry capsules and landers, direct sterilization must be accomplished and maintained to the 10^{-4} contamination probability. Since there may be a burden of 10^9 micro-organisms in and on a spacecraft that is assembled under suitable clean room conditions, this requirement means that the micro-organism population must be reduced by a factor of 10^{13}. Among the possible sterilization procedures are the application of dry heat at 135°C for 24 hr, exposure to ethylene oxide (12% ethylene oxide mixed with 88% freon-12) for 18 hr at 70° to 100°F, and 30 to 50% relative humidity, and exposure to radiation doses of 1.2×10^7 rad. Only the first of these, namely, dry heat sterilization, is presently deemed acceptable.

Therefore, a design objective is to produce a lander that can be completely sterilized by the application of dry heat. However, certain components and subsystems of the lander may be sensitive to the thermal environment necessary for dry heat sterilization, so that removal of the thermolabile components and their subsequent sterile reassembly would have to be utilized. The lander must be heated to 135°C throughout without excessively heating any particular portion. Provisions must also be made for maintaining and assaying sterility during handling and checkout of the lander. The subsystems that present the most difficult problems are solid propellant systems, pyrotechnics, and batteries. The first two present safety hazards during the dry heat sterilization, which therefore must be done in a remote area. Although propellants and pyrotechnics have been developed which are amenable to dry heat sterilization, the arming, safing, and ignition of these devices require a serious development program. Among batteries, only Ni-Cd batteries and some thermal batteries have thus far been demonstrated to be sterilizable by the application of dry heat.

Launch Vehicle Considerations

The size and weight of a planetary entry vehicle are determined to a large degree by the capability of the launch vehicle that injects the entry vehicle and its flyby bus or orbiter bus into an interplanetary transfer trajectory. (An orbiter bus can perform measurements and mapping for a long time, whereas a flyby bus remains in the vicinity only for a short time.) Considering transfer trajectories with near-minimum departure velocity (i.e., near maximum injected weight), the injection velocity for Mars missions ranges from 37,400 to 40,700 fps. Figure 1 shows the nominal injected payload (including ascent shroud) capability of various candidate launch vehicles for an eastward (90° azimuth) launch from Cape Kennedy.[6] Actual design payloads will be somewhat smaller, because launch azimuths other than 90° must be accommodated. (Current range safety requirements at Cape Kennedy constrain the launch azimuth to between 90° and 114°; this constraint eliminates some launch opportunities or forces the use of a dogleg maneuver after launch with the associated degradation of injected-weight capability.) The capabilities of these launch vehicles may be significantly increased in the future by increasing the propellant load or upgrading the propellant combinations used in any or all of their stages.

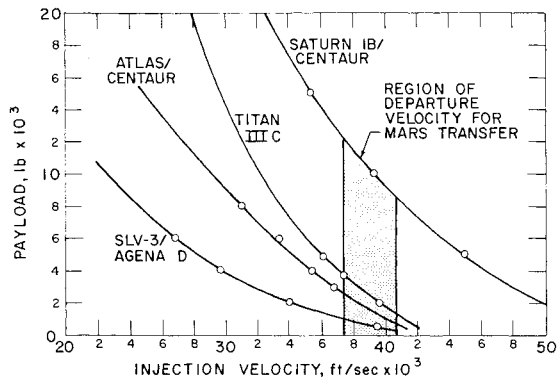

Fig. 1 Injected payload capability for different launch vehicles.

Injected-weight capabilities of at least 3000, 1400, and 650 lb seem to be necessary to accomplish the long-lifetime lander mission, the short-lived lander mission, and the atmospheric probe mission, respectively. If an orbiter rather than a flyby bus is used in conjunction with the entry vehicle, these injected-weight requirements become 7500, 3000, and 2300 lb, respectively. The ascent shroud dimensions usually impose a limit on spacecraft diameter. For the vehicles in Fig. 1, the maximum shroud diameters with no hammer-heading are 260 in. for Saturn, 120 in. for Titan III, 123 in. for Centaur, and 60–65 in. for Agena. In general, to provide adequate clearance under the dynamic launch environment, the payload envelope for the larger boosters must be about 10–15 in. smaller than the shroud dimensions.

Launch Window and Trajectory Considerations

A launch window from Earth to Mars occurs every 25.6 months. Since the orbit of Mars is neither circular nor coplaner with the ecliptic plane, the minimum injection energy over these launch windows varies with launch opportunity. Approximate repetition of the same absolute Earth-Mars geometry every 15 yr or 7 synodic periods results in a cyclic recurrence of the injection energy requirement. Within this 15-yr metonic cycle, the absolute minimum injection energy requirements occur next in 1971 for type I transfer trajectories and in 1969 for type II trajectories.[7] (Types I and II traverse heliocentric angles less than and greater than 180° between departure and encounter, respectively.)

Within a given launch window and among launch windows, there are considerable variations in flight-time-to-encounter and the corresponding communications distance to Earth.[8] For example, the communications range varies from 8×10^7 to 4×10^8 km, while the time of flight typically varies from four to ten months and can exceed thirteen months. Approach velocity and direction and dispersion in the impact parameter also vary widely. [The impact parameter, which is the aiming point or unperturbed passing distance from the planet for the interplanetary transit vehicle (Fig. 2), is related to the periapsis radius r_P by $B = r_P (1 + 2\mu/r_P V_\infty^2)^{1/2}$.] Approach velocities can vary from 8000 to 33,000 fps, and the corresponding entry velocities range from 18,000 to 37,000 fps. In addition to affecting entry velocity, the approach velocity determines 1) the dwell time in the vicinity of the planet for a flyby bus and thus the time available for scientific experiments from the bus, 2) the time available for communications between a lander and Earth via a relay link on the flyby bus, and/or 3) the retropropulsion requirements necessary to place an orbiter bus into orbit about Mars.

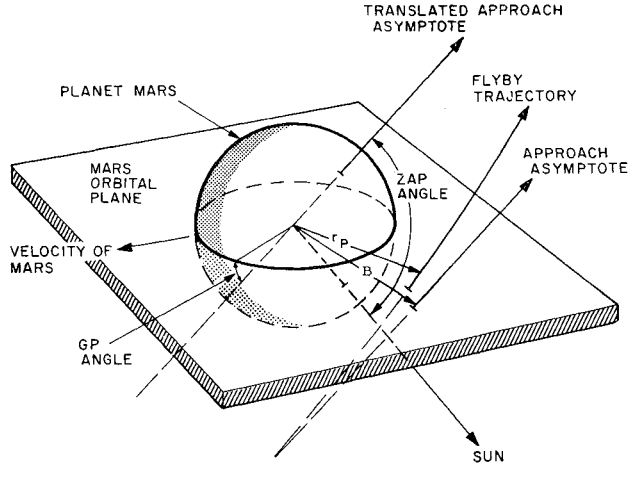

Fig. 2 Mars encounter trajectory geometry.

The approach direction is defined by the *ZAP* angle, the *GP* angle, and the orbital plane of Mars (Fig. 2; the shaded region indicates the dark side of the planet). The *ZAP* angle is the angle between the approach asymptote and the planet-sun line. Since the heliocentric velocity of the spacecraft is smaller in magnitude than that of Mars, the spacecraft is overtaken by the planet and therefore appears to approach from the planet's leading edge relative to its motion about the sun. For typical type I trajectories, the spacecraft approaches from the planet's sunlit side, and the *ZAP* angle varies between 70° and 165° for different launch times and launch windows. For typical type II trajectories, the spacecraft approaches from the dark side and the *ZAP* angle varies between 30° and 120°. The requirement for lander entry, descent, and planetary impact to occur within sight of the Deep Space Instrumentation Facility (DSIF) communications sites on Earth limits the *ZAP* angle to between 80° and 165° if steep entry trajectories are to be flown. (Shallow entry angles result in a larger impact point dispersion, and errors in landing point location may degrade the results from life detection experiments; entry angles less than −20° may result in skipout.) Missions requiring visible spectrum optics during entry and descent should most probably be directed to impact on the sunlit side of the planet; for steep entry angles, this calls for *ZAP* angles between 100° and 260°. Finally, to satisfy possible relay geometry requirements for reasonable communications between the lander and the flyby bus or orbiter link to Earth, *ZAP* angles between 60° and 120° are desirable. In general, *ZAP* angles near 90° provide the best solution to all of the previous requirements.

The *GP* angle is the angle between the approach asymptote and the planet's orbital plane. For most feasible transfer trajectories, the *GP* angle lies between +30° and −30°. The approach direction and the selected flyby inclination also define the period of occultation sustained by a flyby bus. Occultation of the sun or the star Canopus, which are used as attitude references, or occultation of Earth for command and communications, can occur during or immediately following planetary encounter. A sustained occultation of one or more of these bodies places serious limitations upon the capability of a flyby bus.

The final trajectory characteristic of interest is the impact parameter, or planetary miss distance, *B*. To obviate the necessity for sterilizing a flyby or orbiter bus, the interplanetary trajectory could be biased to a safe value of *B* (see Fig. 2). Entry vehicles could be directed to the planet by timely separation from the flyby or orbiter bus and the subsequent application of an appropriate velocity increment. (In addition, deflections of the bus trajectory itself have been studied as well.) The accuracy with which the entry vehicle achieves a preselected landing site will decrease as *B* is increased. The trajectory of the spacecraft can be corrected a number of times during the long interplanetary flight, but each such correction may require a rather complex maneuver and a midcourse engine burn. One to three such corrections are usually considered. The first reduces the dispersion due to

ascent and injection guidance errors; subsequent corrections refine the first and allow removal of other effects, such as solar pressure and meteorite impact. The remaining 1σ dispersion in B after the first correction may be as large as 15,000 km; after two corrections, 1000 km; after three corrections, it can be reduced to as low as 150 km. The total 1σ dispersion in landing point due to errors in spacecraft position at lander separation and errors in the magnitude and direction of the subsequently applied velocity increment can be kept in the range of 180 to 300 km.

Communication Considerations

Communication with Earth could be accomplished by either direct link from the lander to the DSIF stations on Earth or by relay link through the flyby bus or orbiter bus to the DSIF stations on Earth. A host of factors govern communications weight for any given mission. Weights of some components vary with transmitter power, but others do not. The simplest communication system for a relatively low data-rate atmospheric probe could be designed for about 15 lb, whereas the system for a long-lifetime lander may weigh over 200 lb.

During the lander vehicle's entry and descent, relay communications may prove to be the more practical. As an alternative, data can be gathered and stored during descent and then transmitted after impact via direct link to Earth. All communications may be interrupted temporarily during planetary entry by the plasma sheath that surrounds the lander, severely attenuating transmitted signals. After impact, either direct or relay communications links could be used. The performance margin M of a communications system is the degree to which the received signal level exceeds the operating threshold level. It is given by

$$M = P_t G / K_n B_r F L_c L_s L_a R_{snt} \qquad (1)$$

where P_t is the transmitted power (watts); G is the total antenna gain; K_n is the noise power density (watts per cycles per second); B_r is the receiver bandwidth (cycles per second); F is the receiver noise figure; L_c is the total circuit loss; L_s is the free space loss; L_a is the sum of atmospheric losses (Earth and Mars); and R_{snt} is the threshold signal-to-noise ratio. A brief discussion of these factors is given below for both the direct and relay links.

Direct link system

A summary of the capabilities of the DSIF stations on Earth[9] is presented in Table 1. For the direct link system, P_t from a lander is limited primarily by the availability of proved power amplifier devices at the required S-band frequency. Devices are presently available at $P_t \leq 20$ w, and power tubes yielding up to 100 w are under development. The transmitter power is further constrained by the lander power source, which becomes an acute problem for long missions. Special precautions are necessary to prevent corona and voltage breakdown in cables, connectors, and antennas if high transmitter power levels are used in the tenuous Martian atmosphere; the antenna might be placed within a pressurized or evacuated radome to assure against the occurrence of these phenomena. The total gain G is the product of the gain of the 210-ft DSIF receiving antenna (60 db is worst case) and the gain of the lander transmitting antenna, which is limited primarily by the size and antenna-pointing capability of the lander. (If the 210-ft dishes are not available for any reason, the 85-ft dishes should be considered as well.) A practical upper limit on antenna diameters of 8 ft (or more) appear practical for landers, resulting in a maximum on-axis gain of 32 db. Polarization losses should also be included in G (3 db if linearly polarized transmission is used). The noise power density K_n is determined by the receiver noise temperature (33°K worst case for the DSIF) and is -183.2 dbm.

The total power required to establish a synchronous detection communication link is the sum of that required for the carrier channel, the synchronization channel, and the data transmission channel. Equation (1) must be employed independently for the three calculations. The data noise bandwidth is equal to the bit rate, but, due to the mixing process in the receiver, the synchronization and carrier channel effective noise bandwidths are twice the actual bandwidth. The effective noise bandwidth normally used is 5, 10, or 20 cps. For typical S-band operation, the receiver noise figure F is 3 or 4 db.

The receiving circuit loss in the DSIF is less than 0.1 db, whereas the transmitting circuit loss is typically 1 or 2 db. The over-all circuit loss L_c is therefore taken to 2.1 db. Free space loss L_s (transmitted energy that misses the receiving antenna) varies directly with the squares of frequency f and communications range R so that

$$L_s = 32.46 + 20 \log_{10} f + 20 \log_{10} R \qquad (2)$$

where L_s is in decibels, f is in megacycles, and R is in kilometers. Atmospheric attenuation loss L_a is negligible for frequencies below 10^4 Mc except during the high-velocity portion of the entry during which plasma attenuation causes a temporary blackout.

The R_{snt} requirements vary for the three separate power calculations.[11, 10] The carrier channel signal-to-noise ratio should be at least 6 db for adequate performance,[12–14] whereas for the synchronization channel it should be approximately 10 db, and for the data channel the requirement varies with the modulation technique used and the desired bit error probability as shown in Fig. 3.[15, 16] At least 2 db must be allowed in each case to account for off-theoretical performance.

The PCM/PSK/PM S-band system used for direct transmission to Earth allows bit rates dependent upon the lander's P_tG product and the range involved. Figure 4a shows the power gain product required for transmission at various bit rates and interplanetary ranges. The worst case gain of the 210-ft DSIF receiving antenna (60 db) and a carrier loop bandwidth of 5 cps were used in the calculations. Therefore, P_tG involves only the transmitting antenna gain explicitly.

Relay link system

Relay communication links could be designed at a variety of frequencies. Since the required P_tG varies directly with f^2, it is desirable to use as low a frequency as possible, but the maximum practical antenna diameter imposes a lower limit on f. Figure 4b shows the power gain product required for a PCM/PSK/PM modulated relay communications system for various bit rates as a function of R for a carrier frequency of 1000 Mc and receiver loop bandwidth of 100 cps. [The

Table 1 Deep Space Instrumentation Facility Characteristics

	Transmit	Receive
f, M_c	2110.00–2111.83	2290.00–2293.33
	2111.83–2114.83	2293.33–2296.67
	2114.83–2120.00	2296.67–2300.00
Feed location	Cassegrain	Cassegrain
P_t, kw: Goldstone, Calif.	100	...
Woomera, Australia	10	...
Johannesburg, S. Africa	10	...
Noise temp, °K	...	28 ± 5
Noise bandwidth, cps	...	2–250
Antenna diam, ft	85	210
Gain, db	51 ± 1	61 ± 1
Feed line loss, db	0.4 max	0.2 max
Beamwidth, deg[a]	0.35	0.10

[a] Beam can have either left-hand or right-hand circular polarization.

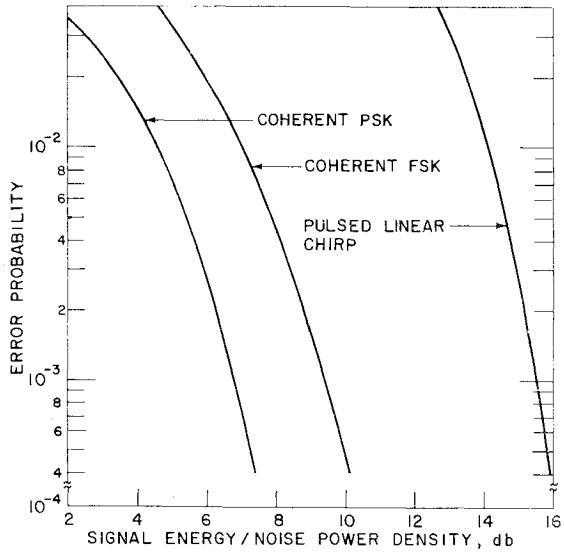

Fig. 3 Signal-to-noise ratio requirements as a function of bit error probability for different binary modulation schemes.

antenna gain is taken to be the sum of the transmitting and receiving antenna gains (in decibels) less the appropriate pointing losses.] This system is efficient, but it has serious drawbacks as a relay communications link. The time required for a phase-lock receiver to acquire and lock onto the received signal varies upward from 10 sec, depending on the receiver loop bandwidth (for typical relay links, 100 cps offers a reasonable compromise between acquisition time and receiver sensitivity).[17] This time reduces the time available for data transmission between exit from blackout and vehicle surface impact. For small vehicles without descent retardation systems (such as light-weight atmospheric probes) or for larger vehicles that have experienced a failure in the retardation system, this time loss may be very serious, and it will be aggravated if a very low density atmosphere is encountered on Mars.

A second problem, peculiar with a relay link, is the wide range of lander-to-flyby look angles which must be accommodated; this variation necessitates the use of a narrow-beam antenna with its attendant complex erection and aiming system, or the use of a broad-beam antenna on the lander, which creates a potential multipath problem for modulation schemes such as PCM/PSK/PM. Several different modulation schemes have been proposed to overcome this multipath problem. The most practical of these appears to be a pulsed linear chirp technique,[18] which uses the same technique employed in pulse compression radar to avoid interference between signals arriving at the receiver via different transmission paths. A penalty of approximately 9 db is incurred in R_{snt}, however (Fig. 3).

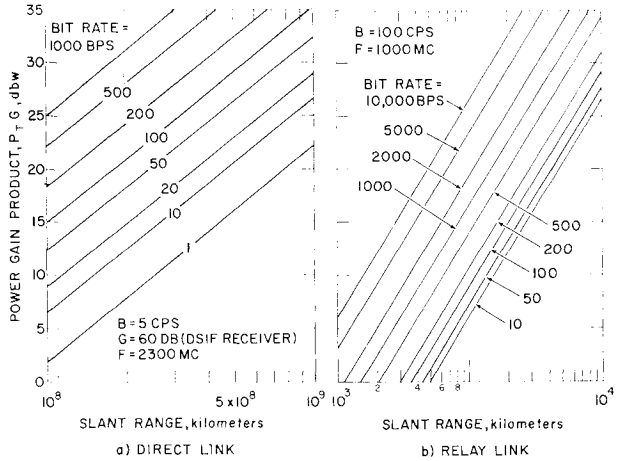

Fig. 4 Transmitter power-antenna gain product requirements for direct and relay link communications systems with different bit rates as a function of communications range.

Power Sources

The selection of a power source for Mars landers is restricted by the requirement for sterilization; the dry heat technique provides a destructive environment for many components. The occasional cloud cover on Mars also limits the use of solar energy converters as postlanding power sources. Open cycle (i.e., entailing production of waste products) power sources are undesirable due to possible contamination of scientific experiments. Therefore, the useful types of power supplies are sterilizable batteries, fuel cells, and radioisotope or pure nuclear thermoelectric or thermionic generators (RTG). Each is useful in a distinct regime as shown in Fig. 5. Among batteries, Ni-Cd batteries have been shown to be dry heat sterilizable,[19] but other types show promise of higher specific power output than the present 6–10 w-hr/lb. The regenerative fuel cell (closed cycle) appears to be competitive for missions exceeding 8 to 10 hr and provides from 15 to100 w-hr/lb, depending upon the magnitude and duration of its use.[22] Very little work has been done to develop a sterilizable fuel cell, but there appears to be no basic difficulty in doing so.

The RTG, which provides a power source rather than an energy source, is essential for missions exceeding one month.[21, 22] The RTG provides 2–4 w/lb but may create a severe thermal control problem, because the thermoelectric converter operates at 1500°F and could require large radiation cooling surfaces to maintain a reasonable internal temperature environment for the other lander subsystems. The radioisotopes curium 224 and plutonium 238 appear best suited for this application, which requires a long half-life. Neither isotope requires excessive shielding, but both present an availability problem. RTG development now underway is expected to be sufficiently advanced by 1969 to be useful in providing power sources for the early Mars landers.[23]

Mars Entry Problem

Mars Atmospheric Models

Atmospheric characteristics play a strong role in establishing entry vehicle design criteria. Earth-based observations of Mars have yielded useful but fragmentary data that leave

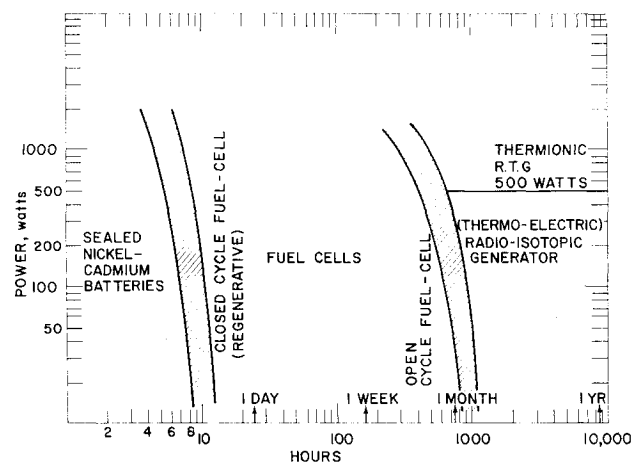

Fig. 5 Projected power-time operating regimes for sterilizable power sources.

considerable uncertainties in these characteristics. Many atmospheric models have been postulated; for design purposes, the worst combination of conditions is often chosen. The atmospheric characteristics that most heavily influence the lander design are surface pressure, atmospheric composition, and vertical structure of the atmosphere. The surface pressure determines the maximum vehicle ballistic parameter (m/C_DA, slug/square foot) required to achieve suitable entry deceleration. High wind velocities can result in high landing impact velocities, even though the vertical descent velocity component is small. Atmospheric composition affects radiative heat transfer during entry, and vertical structure (e.g., scale height) governs peak deceleration loads.

Regarding surface pressure (p_{surf}) the most recent estimates by Kaplan, Munch, and Spinrad[24] (based on spectroscopic observations) indicate that it may be as low as 10 mb (i.e., 10^{-2} atm). Heretofore, there had been general concurrence (e.g., the survey of Rasool[25]) that the nominal p_{surf} was 85 mb, with a minimum value of 41 mb (Schilling).[26] Early estimates on the correlation of the CO_2 concentration and p_{surf} were made by Grandjean and Goody[27] based on the analysis of Kuiper's[28] spectroscopic observations (1947), and indicated p_{surf} as low as 13 mb for a 100% CO_2 atmosphere. The possibility that p_{surf} is as low as 10 mb is a key factor affecting the design of entry vehicles for Mars.

A summary of observations of moving cloud formations (wind velocity) is given by DeVaucouleurs.[29] The peak velocity of the observed yellow cloud systems is 91 fps. The altitude of these clouds is estimated to be on the order or 20,000 ft.[25] Recent NASA-sponsored lander studies[30] have considered winds in the low-pressure model atmospheres as high as 200 fps.

The possibility of high winds is extremely important, because the additional nonpayload weight necessary to attenuate the impact loads increases as the square of the impact velocity. Recent spectroscopic observations[24] indicate an abundance of CO_2 in the atmosphere, 55 ± 20 m-atm. From this the mole fraction of CO_2, X_{CO_2} can be deduced as a function of the surface pressure. The remainder of the gas in the atmosphere probably is nitrogen and/or argon.[24] Figure 6 shows that the X_{CO_2} becomes large in the low-pressure models; hence the molecular weight (M) of the atmosphere is also higher. Various CO_2-N_2-A mixtures have been selected for entry studies; e.g., Haurlan,[30] Spiegel,[31] and Levin, Evans, and Stevens.[32] A summary of infrared radiometric observations[25] indicates surface temperatures of 220° to 300°K, depending on latitude and season. The temperature gradient through the troposphere should be close to the adiabatic lapse rate, since the atmosphere has a negligible water content. The temperature in the stratosphere is estimated to be as low as 130°K (the solidification temperature for CO_2). Several recent model atmospheres are summarized in Table 2,[30] wherein the temperature gradient in the troposphere is assumed linear, and above the tropopause the temperature is assumed to be constant up to the entry altitude. The molecular weight (M) is presently considered to be constant

Table 2 Interim low-pressure model atmospheres for Mars[a] (g_c = 12.3 ft/sec² for each)

Property	Model atmosphere				
	G	*H*	*I*	*J*	*K*
p_{surf}, mb	11	11	15	30	30
psf	23.0	23.0	31.3	62.6	62.6
T_{strat}, °K	130	230	180	130	230
X_{CO_2}	0.648	0.648	0.433	0.105	0.105
X_A	0.352	0.352	0.322	0.130	0.130
X_{N_2}	0	0	0.245	0.765	0.765
$\mathfrak{M}$	42.6	42.6	38.8	31.3	31.3
h_{scale}, kft	22.2	39.3	33.7	30.2	53.5

[a] E. Framan, Ref. 30, Appendix B.

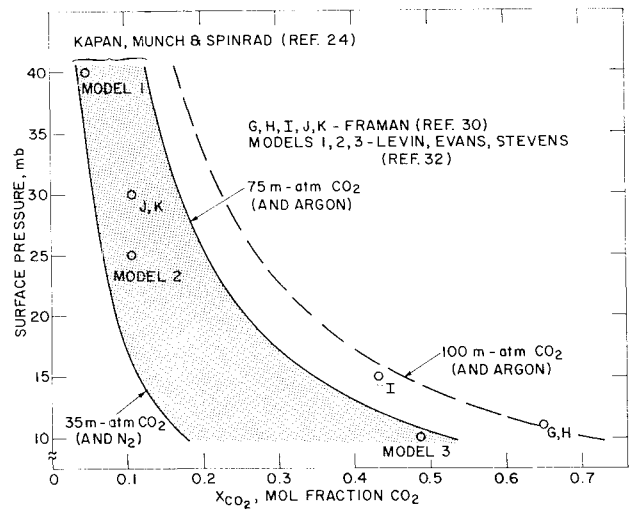

Fig. 6 Variation of mole fraction of carbon dioxide with surface pressure.

with altitude up to the entry altitude at which the first significant thermal effects of entry occur.

The smallest scale height in Table 2 is close to the value for Earth; hence, for that atmosphere, peak loads could be simulated by Earth flight tests duplicating the entry velocity, flight path angle, and the drag characteristics of the entry vehicle. Similarly, Earth flight test simulation of peak convective heating is also possible, since ground tests and theory indicate that composition has only a small effect on the convective heating over the range of entry velocities (V_e <29,000 fps) presently being considered for unmanned missions. Since only p_{surf} and X_{CO_2} are presently correlated, modifications and/or additions to these models will continue as more data become available, e.g., Ref. 32.

Entry Vehicle Design Considerations

The possibility of encountering very low surface pressures makes high-drag configurations essential for a lander. Vehicle stability (both hypersonic and subsonic) is an important factor, because oscillations affect the drag characteristics and communications (due to antenna orientation changes with angle of attack). These factors, as well as the heat protection requirements, effects of drag deceleration loads and configuration on structure requirements, and the parachute or other auxiliary drag devices and impact attenuation systems for landing, have recently been reviewed by Roberts[33] and are discussed below.

Ballistic parameter (m/C_DA) requirements

The surface pressure sharply influences the m/C_DA requirements, as shown in Fig. 7, for vertical entry for several mission criteria. The m/C_DA referred to here is the nominal hypersonic value at zero angle of attack (α = 0); the actual value depends on the α motions and vehicle shape, as discussed later. The uppermost curve represents the maximum allowable m/C_DA for a blunt entry vehicle, which could communicate for 10 sec (allowing 10 sec for acquisition of the telemetry signal) following the communication blackout due to peak ionization. Electron density studies in various atmospheres[34] indicate that the blackout problem is grossly similar to that for Earth, and exit from blackout is likely when the velocity has decreased to 8000 fps.

Since Mars rotates at about the same rate as Earth, the atmosphere has a speed of about 800 fps at its equator. A vehicle entering from space may not acquire the tangential speed of the atmosphere if its m/C_DA is too high. For a vehicle entering the atmosphere normally (γ_e = −90°), the

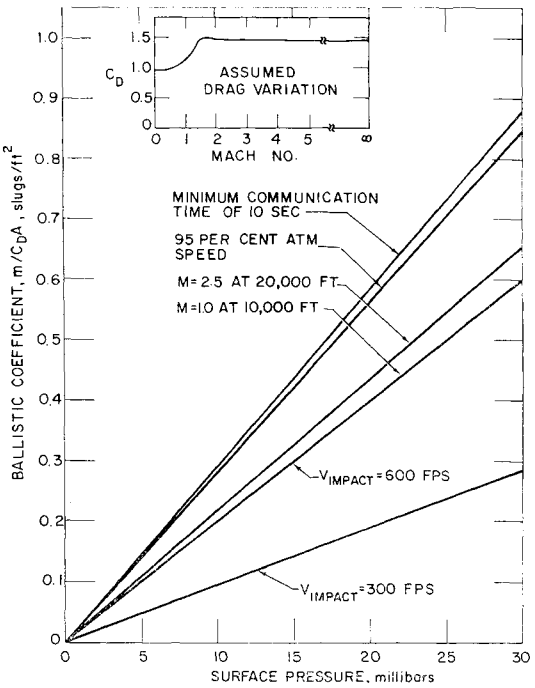

Fig. 7 Effect of surface pressure on the required entry vehicle ballistic parameter for different deceleration criteria.

velocity acquired by the vehicle due to a side wind is given approximately by $V_y = V_w [1 - \exp(-C_D A p/2mg)]$. The curve labeled "95% of atmosphere speed" in Fig. 7 reflects the requirement for an entry vehicle to acquire 95% of the rotational speed of the atmosphere prior to impact at the equator. The requirements for decelerating to Mach 2.5 at 20,000 ft (where a supersonic parachute could be deployed) and to Mach 1.0 at 10,000 ft (the limit for subsonic parachute deployment or for a probe without a parachute where subsonic terminal flight is desired) are also shown. The most stringent demands for low m/C_DA result from missions requiring landing and survival without auxiliary decelerators, thereby requiring relatively low impact velocities (from 600 to 300 fps; see two lower curves).

It is seen that, if $p_{surf} = 10$ mb, all missions require m/C_DA's of less than 0.3 slug/ft². An m/C_DA of as low as 0.1 slug/ft² may be necessary if it is required that V_{impact} speed ≤ 300 fps even if a parachute system malfunctions. The allowable m/C_DA can be increased by using a shallower entry angle, since the permissible m/C_DA varies roughly with $(\sin\gamma_e)^{-1}$. However, even if the nominal entry angle is shallow, the possible failure mode of vertical entry is likely to be a design requirement for the initial missions.

The launch vehicle shroud dimension constraints coupled with the requirement for low m/C_DA may further limit the allowable entry vehicle weight (W_e) as the maximum entry weight is $W_e = 25\ (m/C_DA)C_DD^2$. With entry vehicle diameter (and drag area) limited by shroud diameter, the allowable W_e for a given m/C_DA can be adjusted only by varying C_D (for fixed geometry vehicles). The large diameter of the Saturn provides ample contingency for planning a heavy lander mission in the event that the surface pressure is as low as 10 mb.

Entry flight regimes

The combination of the atmospheric models of Table 2 with mission requirements results in the definition of flight regimes within the Mars atmosphere as depicted in Fig. 8. The zones where peak Reynolds number (Re) peak dynamic (load pressure(q_∞), and peak convective heating ($\dot{Q}_c$) occur are indicated by the shaded regions). A 10-mb surface pressure on Mars is equivalent to 100 kft on Earth, and thus important entry events are seen to occur in the equivalent altitude range of 160 kft. The range of peak radiative heating ($\dot{Q}_r$) lies between peak q_∞ and peak $\dot{Q}_c$, depending on the gas composition. Note that 10% of peak $\dot{Q}_c$ occurs at equivalent altitudes between 290 and 300 kft. [The occurrence of these events can be predicted using simplified trajectory (isothermal atmosphere, straight line trajectory) relationships,[35] wherein any function in the form of $\rho^a V^b$ has a peak when the flight velocity is $V = V_e e^{-b/a}$ and the ambient pressure is $P = -(a/b)(2\ mg/C_DA)\sin\gamma_e$. Stagnation-point $\dot{Q}_c$ has an $a/b \cong 0.16$, depending upon gas composition; $\dot{Q}_r$ has a value of $a/b \cong 0.20$, depending on V_e and gas composition; q_∞ has $a/b = 0.50$; and Re has $a/b = 1.0$.] Peak q_∞ can occur within the troposphere for some of the atmospheres. With respect to turbulent heating, a transition to turbulent flow is expected at altitudes slightly below 200 kft (based on $Re = 300{,}000$ at the sonic point).

The appearance of significant nonequilibrium radiation effects can also be inferred from Fig. 8. (The extent of the nonequilibrium radiation region is governed by various relaxation processes and is therefore a function of V and p.) At pressures below the line labeled "nonequilibrium radiation dominates," the entire radiating shock layer at the stagnation point is out of equilibrium. This demarcation is based on data,[36] which indicate that for CO_2-N_2 mixtures the depth of the nonequilibrium region behind the normal shock at the stagnation point appears to be 3 to 6 times as large as that for air. The results of Howe and Viegas[37] on the relaxation time for CO_2 behind a normal shock have been used in Fig. 8 to indicate the regime where chemical relaxation effects are significant. At present, the chemistry of the gas mixtures of interest is relatively unknown; but it is apparent that in the altitude region on Mars where significant heat fluxes occur, the flow in the shock layer and the boundary layer is likely to be out of equilibrium. The zone where strong viscous interaction exists[38] has also been identified on Fig. 8. It is apparent that strong vorticity interactions exist especially for small vehicles.

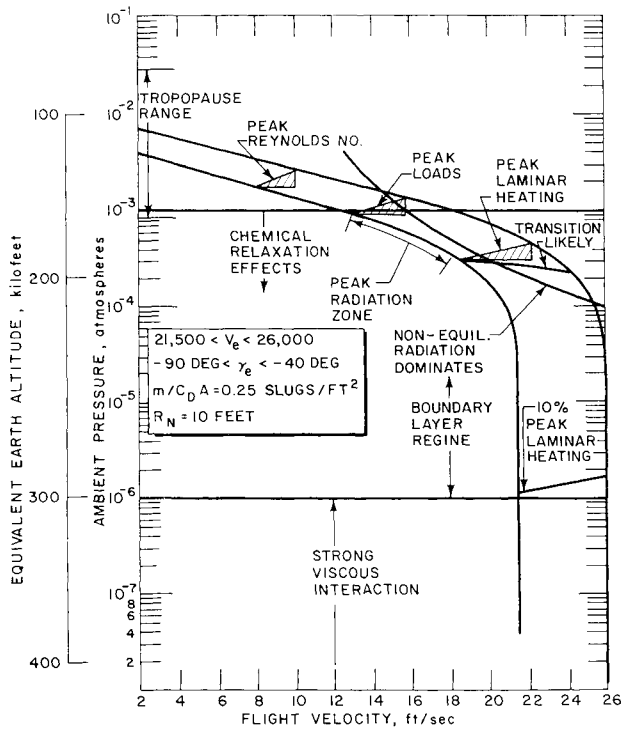

Fig. 8 Mars entry flight regimes for a typical lander vehicle.

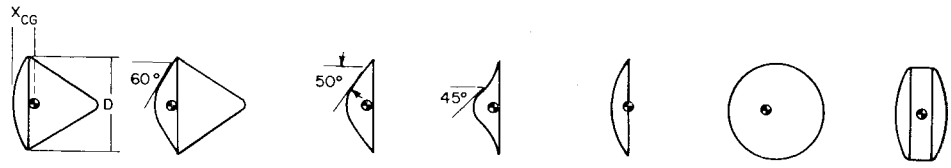

CONFIGURATION	1	2	3	4	5	6	7
S_N/C_DA	0.65	0.75	0.90	0.75	0.65	2.0	1.8
S_{AB}/C_DA	1.05	1.25	0.70	0.65	0.60	2.0	—
TRIM	1-POINT	1-POINT	(a)	(a)	(a)	1-POINT	2-POINT
LOW-V STABILITY	POOR	PROBABLY POOR	PROBABLY GOOD	PROBABLY GOOD	GOOD	POOR	PROBABLY POOR
X_{CP}/D(b)	0.85	0.75	0.60	0.65	0.85	0.50	0.85
REFERENCES	42,43,44,45	42	40,41,46	33,40,41,47,48	40,41	33,39,49,50	39

a) POSSIBLE TRIM PROBLEM AT α=180 DEG. b) CENTER-OF-PRESSURE LOCATION α=0 DEG (NEWTONIAN).

Fig. 9 Mars entry vehicle configurations.

Aerodynamic stability requirements

The stability requirements and resultant problem areas stem in part from the nature of the Mars atmosphere and in part from mission requirements. For example, an entry vehicle can be integrated with a flyby spacecraft (similar to Mariner 4), which has the necessary guidance and control systems to assure a successful planetary encounter. The entry vehicle will most likely be enclosed within a sealed canister insuring a contamination barrier between it and the flyby bus. Furthermore, if the flyby bus is unsterilized, it must either fly a biased trajectory to insure that it does not impact the planet or it must be deflected to avoid impacting the planet. In the former case, the entry vehicle must have its own propulsion system and a thrust vector control (TVC) system. Several approaches to the TVC are possible such as active or spin systems. In the event that the entry vehicle is spun, upon separation from the bus, the initial entry conditions at the planet will depend on the attitude of the vehicle when it is spun and whether or not it is despun prior to start of entry. Depending on the separation approach, the entry angle of attack (α) can be larger than 90° (or could be small) and the vehicle could have a high spin rate. The entry vehicle may have to be despun prior to entry if the magnitudes of the moments of inertia about the pitch, yaw, and roll axes are similar to avoid the possibility of spin axis transfer resulting in large pitch rates at entry.

To assure that the vehicle will right itself sufficiently prior to peak heating and loads, regardless of entry attitude and the various combinations of pitch, yaw, and roll rates, the vehicle configuration must have a single stable trim point (at $\alpha = 0$) and good stability characteristics. Configurations that have received extensive study for the low-pressure model atmospheres are summarized in Fig. 9. The remarks relating to low-speed stability, to trim problems at $\alpha = 180°$, and structural weight are based on references indicated in Fig. 9. In some instances where data are incomplete or unpublished, the low-speed-stability performance is an estimate only. The local drag coefficients, S_N/C_DA and S_{AB}/C_DA, refer to those portions of the total surface area which experience high heating and low heating, respectively; these parameters relate to heat shield and structural weight requirements, as discussed later.

In the absence of a parachute system or in the event of parachute failure, it is extremely desirable to have a vehicle that is statically and dynamically stable throughout the entire Mach number range, so that the antenna orientation remains relatively fixed (for more favorable gain characteristics, lower transmitter power level, and alleviation of multipath effects). Large α oscillations would also hinder data gathering and interpretation. Tests[40] indicate that high-drag vehicles can be designed to be dynamically stable at subsonic speeds, and the configurations without afterbodies exemplify a plausible approach to this.

A further consideration is the variation in drag coefficient with angle of attack. Figure 10 shows the variation of C_D with α as estimated by Newtonian theory for the configurations of Fig. 9. These configurations, which were designed for high C_D at $\alpha = 0$ together with small surface area in order to minimize heat shield and structural weights, show a marked decrease in drag near $\alpha = 90°$ (particularly those without afterbodies). The configurations with afterbodies continue to show fairly low drag to $\alpha = 180°$. The vehicle should have the proper combination of drag and stability to insure a low effective m/C_DA throughout its flight. Changes in drag due to α effects can alter the trajectory significantly, increasing the peak stagnation pressures and heating rates and reducing the altitude at which a parachute could be deployed. Blunt-body studies[42] indicate that the effective m/C_DA is generally 10–20% higher than the value for $\alpha = 0$, depending on the severity of the entry conditions, stability characteristics, inertias, etc.

In view of the preceding considerations, the question of dynamic stability for the blunt, high-drag bodies assumes a position of extreme importance. The dynamic stability criterion of Allen[5] illustrates the divergent aspects of high hypersonic drag and dynamic stability. For stability, it is required that

$$C_D - C_{L\alpha} + (C_{m_q} + C_{m_{\dot\alpha}})\,(l/\sigma)^2 < 0$$

By Newtonian theory, $C_{L\alpha} = 2(1 - C_D)$ at small angle of attack, so that

$$3C_D - 2 + (C_{m_q} + C_{m_{\dot\alpha}})(l/\sigma)^2 < 0$$

For high-drag vehicles for which $C_D \simeq 1.5$, it is of utmost importance to have at least a small favorable $(C_{m_q} + C_{m_{\dot\alpha}})$ and a

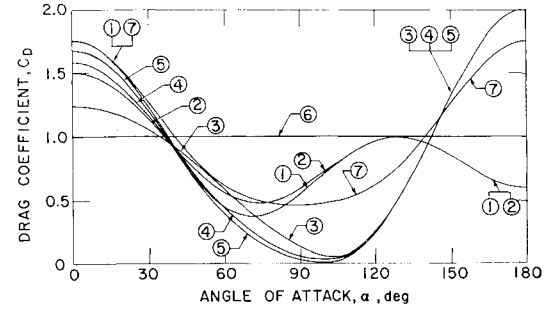

Fig. 10 Drag coefficient variation with angle of attack for the various configurations in Fig. 9.

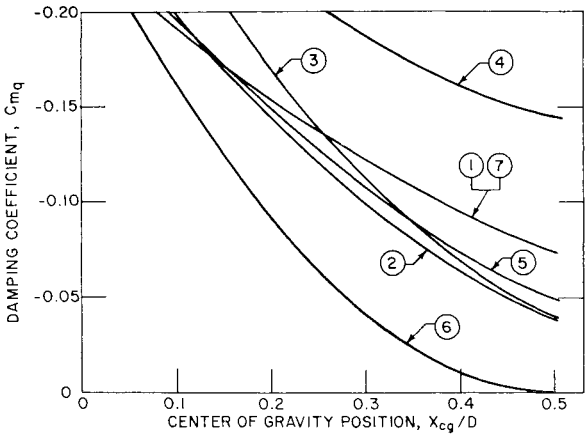

Fig. 11 Variation of damping characteristics with center of gravity location for the configurations in Fig. 9.

large value of l/σ. (The preceding terms are defined in the Nomenclature.)

Several factors combine to make the achievement of adequate stability for the very blunt vehicles quite feasible. First, the initial convergence of α from entry through peak heating and down to peak deceleration is adequate for the blunt vehicles, since the dominating cause of convergence is the rapid rise in q_∞, thus effectively increasing the spring constant of the system. Second, the packaging of the low m/C_DA vehicle is well suited to concentrating the payload about the c.g., thereby making the value of l/σ large, e.g., 3–5. Third, small amounts of damping exist if the c.g. is sufficiently far forward. For example, Fig. 11 illustrates the variation of C_{m_q} calculated by Newtonian theory as a function of c.g. position ($\alpha = 0$) for the high C_D configurations of Fig. 9. The damping term is significant for these shapes and the amplification by the $(l/\sigma)^2$ term provides adequate stability at high Mach numbers. Finally, more detailed analyses of the dynamic stability requirements, such as those by Sommer and Tobak,[52] indicate that α will converge at altitudes below peak q_∞ even for small positive values of the dynamic stability parameter. A parametric study of aerodynamic damping requirements[44] indicates that a value of $(C_{m_q} + C_{m_{\dot\alpha}})$ on the order of -0.10 is adequate to ensure such convergence for configuration 1 of Fig. 9. Gas composition has a significant effect on drag and stability for configurations such as cylinder flares but little effect for blunt, high-drag sphere cones.[53, 54]

Convective heating environment

Atmospheric scale height and composition affect the convective heating. If one chooses a mean nominal value of h_{scale}, the uncertainty between various atmospheres (see Table 2) in stagnation point heating is $\pm 20\%$, since $\dot{Q}_{\text{peak}} \sim \beta^{0.5}$ and $Q \sim \beta^{-0.5}$. For turbulent flow, the uncertainty in $\dot{Q}_{\text{peak}}$ is 30%, since $\dot{Q}_{\text{peak}} \backsim \beta^{0.8}$, whereas the uncertainty in Q is 7%, as $Q \sim \beta^{-0.2}$.

Experimental heat-transfer results for N_2-CO_2 mixtures as well as theoretical studies have been reported widely. Comprehensive bibliographies are given in Refs. 55–59. A partial summary of results pertinent to Mars entry is given in Fig. 12, which shows calculations by Sones[60] for mixtures corresponding to the G, H, I, J, K model atmospheres. Sones used the equilibrium transport properties based on the work of Yos.[61] Similar analytical results by Hoshizaki,[58] Van Tassell,[62] and Fay and Kemp,[59] all based on thermodynamic equilibrium, are also shown for comparison. The results are also expected to hold well for nonequilibrium conditions, since consideration of the limiting case of frozen flow has not led to large differences for velocities of interest. Experimental results for CO_2-N_2 mixtures tend to fall slightly below all of the theories (see the shaded region, which represents results of Collins[57] for 9% CO_2, 90% N_2, and 1% A); similar results are found in Ref. 55.

The analytical results of Sones show only a small effect of composition, but experimental results[57] for mixtures with significant A concentrations (see triangles in Fig. 12) show substantially higher $\dot{Q}$ at high velocities. The reason for this increase is not fully understood but may stem in part from radiative heating effects, because adding A can greatly increase the radiative heating due to the resultant higher temperatures for given flight velocities. Theoretical results[63] indicate as much as a ten-fold increase in the radiation from CO_2-N_2 mixtures at 35,000 fps when A was added. The possibility of large concentrations of A on Mars could affect the convective heating. Theoretical results by Finson and Kemp[64] for pure A indicate Q's about 30% higher than those obtained for CO_2-N_2 mixtures in the low speed range (see Fig. 12). Experimental results[65, 66] show good agreement. The effects of A in the velocity range for peak heating for the 1969 and 1971 Mars missions could increase the convective heating by at most 30% over the CO_2-N_2 mixtures. The results shown in Fig. 12 can be used to ascertain the peak heating rates that are likely to be encountered. By approximate trajectory theory, the stagnation pressure at peak heating is given by

$$P_S \cong -1.6\,(m/C_DA)(\beta \times 10^4)(V/10^4)^2 \sin\gamma_e$$

where $V \cong 0.85\,V_e$. Hence, the peak values of stagnation pressure at peak heating are about 1 atm, and the peak heat rate appears to be 650 $R_N^{-1/2}$ Btu/ft²-sec for m/C_DA = 0.25 slug/ft² and V_e = 26,000 fps.

Radiative heating environment

The formation of cyanogen (CN) behind the bow shock wave leads to large increases in radiation over what is custom-

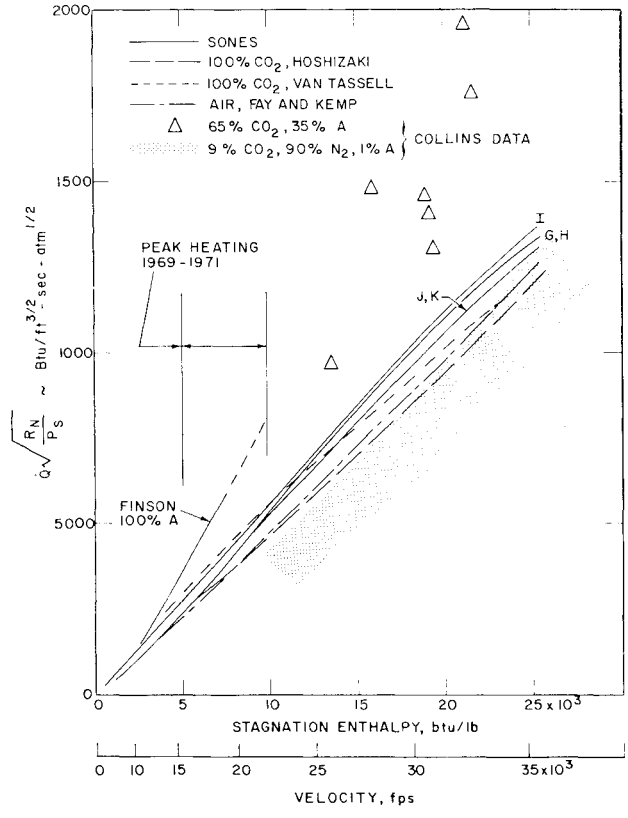

Fig. 12 Stagnation-point convective heating dependence on flight velocity and comparison of theoretical predictions with experimental results.

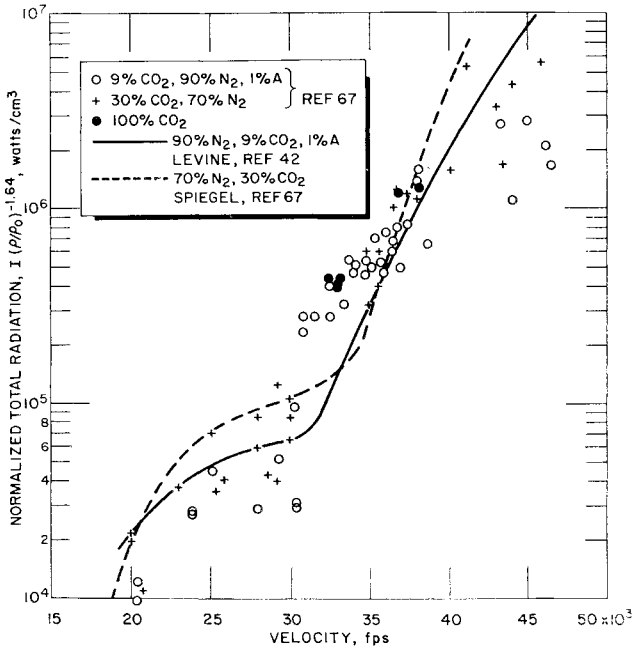

Fig. 13 Comparison of normalized equilibrium radiation intensity data with theoretical predictions.

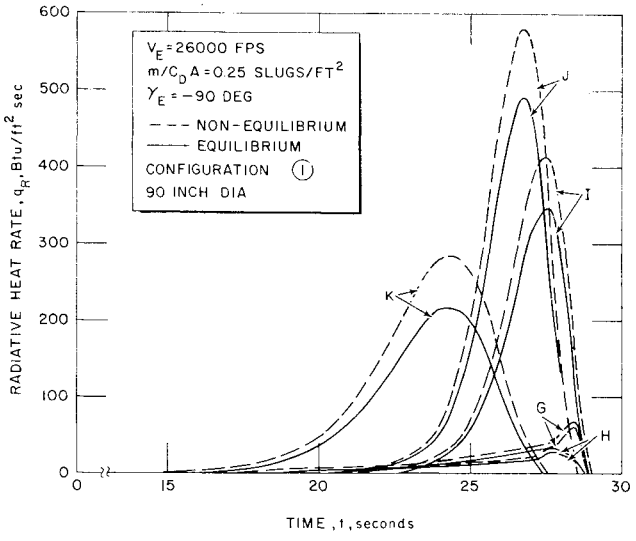

Fig. 14 Stagnation-point radiative heating predictions for a typical entry trajectory for the various model atmospheres of Table 2. The dashed lines represent the total radiation including nonequilibrium effects, whereas the solid lines represent the equilibrium radiative heating alone.

arily observed for Earth entries of comparable velocities. Experimental results[55, 67–69] in N_2-CO_2-A mixtures are summarized in Fig. 13 together with theoretical predictions.[42, 69] The initial rise in radiation is due to the increase in molecular band emission as V increases, but as V continues to increase, the molecular concentrations diminish rapidly due to dissociation; hence, a plateau exists between 25,000 to 30,000 fps. As V increases still further, the concentrations of ionized particles increase rapidly and continuum radiation dominates. Wolf and Horton[63] have shown that the addition of A shifts the plateau region to lower velocities, because the monatomic A raises the gas temperature, leading to dissociation and ionization at lower speeds.

Comparative heat pulses using the method of Levine[42] are shown in Fig. 14 for the five atmospheric models. The J atmosphere (11% CO_2, 75% N_2, 13% A) gives the highest radiative heating. The estimated effects of the nonequilibrium radiation are also indicated. The dashed lines correspond to the sum of the equilibrium plus nonequilibrium radiative heating, whereas the solid lines represent the equilibrium portion only. For shallower γ_e, the relative proportions of nonequilibrium radiation will increase over those shown in Fig. 14.

The results show that the peak equilibrium radiative heating is roughly given by $\dot{Q}_r \cong 50\ R_N$ Btu/ft²-sec for m/C_DA = 0.25 slug/ft² and V_e = 26,000 fps. Scaling the nonequilibrium contributions is more complicated, but, in general, it appears that the peak radiative heating will be less than 1000 Btu/ft²-sec, even for large, blunt landers, if the surface pressure estimates and hence the allowable values of m/C_DA remain low. The peak stagnation convective heating was previously noted as $\dot{Q}_c \simeq 650\ R_N^{-1/2}$ Btu/ft²-sec, indicating a crossover at $R_N \simeq 5$ ft, where the two heating components are equal for the selected conditions.

Heat shield and structure requirements

As a result of the low-surface pressure estimates and the consequent low m/C_DA required under certain mission constraints, the heat shield and structure assume much greater importance than in a conventional ICBM or satellite entry vehicle. For example, the ratio of heat shield and structural weight to entry weight is expressible as $W_{HS}/W_e = (W_{HS}/S)(S/C_DA)(C_DA/m)(\frac{1}{32})$, where W_{HS}/S is weight/total surface area, and S/C_DA is a geometric factor, which can be broken down into surfaces exposed to high heating and loads S_N/C_DA and to low heating and loads S_{AB}/C_DA where $S = S_N + S_{AB}$. The values for configurations 1–7 are given in Fig. 9.

Figure 15 depicts W_{HS}/W_e vs m/C_DA for configuration 1. The range of diameters covers small capsules (~40 in.) short lifetime landers (~60 in.) and long lifetime landers (90–150 in.); the dimensionally smaller vehicles have a more favorable heat shield and structural weight fraction. The weights are based on a composite construction of the nose cap using an ablator bonded to an Al honeycomb substructure. The afterbody consists of a high-temperature Be structure, which serves as the heat shield as well. It is seen that the effects of low surface pressure, requiring a low m/C_DA for certain missions, impose significant W_{HS} penalties. Conversely, at high m/C_DA, payload packaging becomes more difficult for a fixed diameter vehicle if a suitable c.g. position is to be maintained. The c.g. limitations (necessary to meet the requirement for a single stable trim point regardless of entry

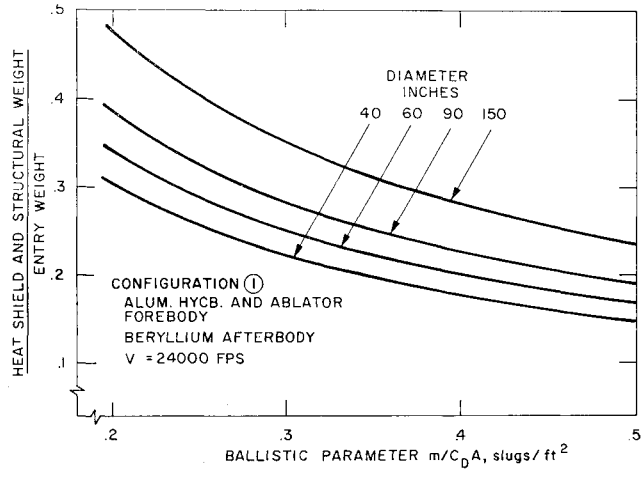

Fig. 15 Effect of entry vehicle ballistic parameter on the required heat shield and structure weight for different diameter but fixed configuration vehicles (configuration 1 of Fig. 9)

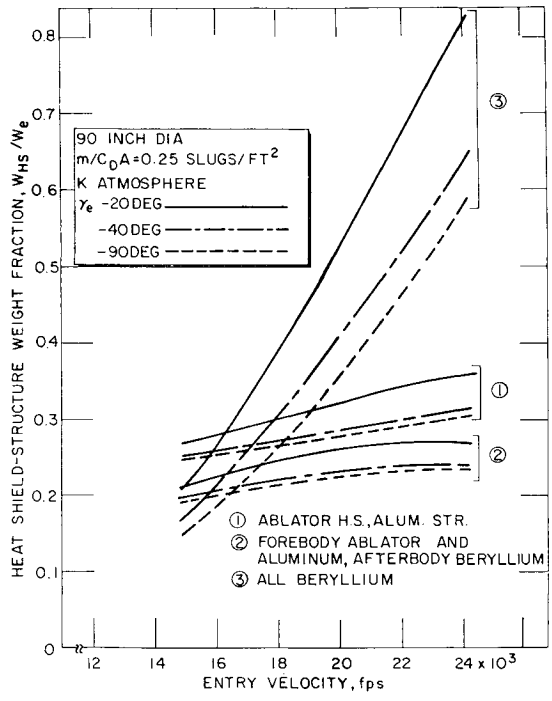

Fig. 16 Effect of entry velocity on the heat shield and structure weight for different entry angles and different heat-shield-structure materials.

attitude) result in a strong interaction between m/C_DA, payload constraints, and vehicle configurations, and this also affects W_{HS}/W_e.

The effects of V_e and γ_e on W_{HS}/W_e are shown in Fig. 16 for two heat-protection and structure schemes and for an all-Be structure. The effects of V_e on W_{HS}/W_e are small for the ablation protected structures, due in part to the radiation heating plateau in the range of 24,000 to 28,000 fps (see Fig. 13) and in part to the increased material ablation efficiency at higher velocities as the heat pulse time is shortened and the enthalpy is increased. Lower integrated heat loads and shorter heating times also explain the beneficial effect of higher γ_e. The all-Be high-temperature structure becomes competitive with ablator designs at velocities below 16,000 to 18,000 fps (approximately the escape velocity for Mars). The influence of atmospheric models on W_{HS}/W_e studied in Ref. 42 indicated only a 15% variation between atmospheres G, H, I, J, K for $V_e = 27{,}000$ fps. Thus, the total variation due to scale height and composition differences may be relatively small if efficient ablators and lightweight structural design techniques are used.

To account for the increase in effective m/C_DA at $\alpha \neq 0$, the m/C_DA at $\alpha = 0$ must be made still smaller, and this reduction in m/C_DA leads to higher W_{HS}/W_e, as indicated in Fig. 15. Reductions of m/C_DA by as much as 20% may be necessary, depending on vehicle configuration, stability, and entry conditions. Furthermore, heating and loads on the afterbody (and possibly the forebody, depending on configuration) are increased by α variations. For example, increasing the spin rate from 10 to 40 rpm at entry ($\alpha_e = 179°$) increased W_{HS} by 15% due to the persistence of large α deep into entry.[42]

Table 3 Laminar arc test results for N_2 and CO_2 mixtures at ~8600 Btu/lb gas enthalpy

Material	Density, lb/ft^3	% CO_2 in mixture	Q,[a] Btu/ft^2 × 10^{-2}	Sample mass loss, %
Teflon	135	0–10	120–134	16.1–16.6
Noncharring epoxy	66.2	0–10	120–134	22.5–23.9
Charring	36.4	0	128	9.1
Epoxy	...	5	120	13.8
Silica	...	10	134	16.0

[a] Q is cold wall heat load at stagnation point for 2-min run.

With respect to vehicle configuration, comparisons[42] indicate that configuration 2 requires 12% more W_{HS} than configuration 1, because the latter has smaller total (S/C_DA). Comparison[47] of configurations 3 and 4 showed that 10 to 30% more W_{HS} is required for the conical configuration. The difference is due to the buckling failure mode of the structure for the cone, whereas configuration 4 is designed for tensile yield and minimum gage considerations.

Configurations 5 and 1 have similar forebody sections and the W_{HS} is 5 to 10% less for 5. The sphere 6 has a relatively heavy heat shield and structure due to its large S/C_DA, but for special missions it is attractive because its drag is independent of α. Configuration 7 represents an attempt to minimize the volume requirement of an entry vehicle; heat shield must be provided fore and aft, since it has two stable trim points, and this results in high W_{HS}.

The problem of dry heat sterilization has a significant influence on the choice of materials. If a composite construction (e.g., an ablator with an Al substructure) is used, the thermal expansion coefficients must be compatible in the sterilization temperature range. At the same time, during interplanetary flight, the cold soak requirements for the heat shield may run as low as −100°F.[45] The need for thermal control coatings of high quality to provide for temperature stabilization of the payload during transit to Mars and after separation from the bus is also interwoven with the sterilization problem, since the thermal control coating must survive sterilization without degradation. The use of an RF-transparent heat shield and structure at the antenna location is also an important consideration for many missions. Noncharring ablators and nonmetallic structures would be required for those portions of the vehicle.

The heat shield material should have a high efficiency over a wide range of heating rates. Low thermal conductivity is particularly desirable. Materials that have a liquid phase may be troublesome for the low heat input pulses, since significant material loss could occur from melting and runoff. The performance of charring materials is sensitive to oxygen content and enthalpy levels (which are relatively low for early missions).[70–72] Table 3[70] summarizes test results on the effects of CO_2 concentration on material performance. The charring material (epoxy silica) appears to be significantly affected, whereas the noncharring materials display little effect. With the likelihood of large concentrations of CO_2 in the atmosphere, it would be desirable to have a material insensitive to oxidation effects. The shear levels expected during entry are a strong function of the m/C_DA and hence of the estimated range of surface pressure. Since the uncertainties in surface pressure could result in a pressure as large as 50 mb, it would be wise to develop materials that can handle the shear stresses for vehicles designed for such denser atmospheres with peak laminar shear stresses as large as 25 psf. The material must also be opaque to the radiation heating and should have a high heat of vaporization to insure good performance for heat pulses that contain a large amount of radiation. Still another major consideration is fabricability, since the heat-shield thickness may be as low as 0.2 in. for an 8-ft-diam vehicle. Materials with rheological properties or those that can be molded directly to the structure are clearly desirable. Other concepts, such as an integral heat-shield and structure utilizing reinforcements, may alleviate a number of the fabrication and thermostructural problems. Finally good mechanical properties would be advantageous because of the aeroelastic aspects of lightweight entry vehicle structures.

Descent parachute system requirements

The possibility of encountering low surface pressures on Mars has led to increased emphasis on parachute deceleration systems. Recent developments[73, 74] in supersonic parachutes have indicated a solution to the stability problem, but Mach number limits are imposed by aerodynamic heating and loading. The ambient temperatures at low altitude can be as high as 260°K, and since the ratios of specific heats ($\gamma = c_p/c_v$) for all the atmospheric models suggested are close to 1.4, the maximum allowable Mach numbers are about 3 for Nylon and 4 for Nomex fabrics.

The parachute descent system for small-capsule missions that do not survive impact must be designed to meet descent time requirements necessary to perform experiments and play out the data prior to impact. Single-chute and multiple-chute systems have been considered. The minimum altitude at which the main chute can be deployed is a function of terrain uncertainties and mission requirements. For a low m/C_DA, W_{HS}/W_e is large and parachute system weight is low. At higher m/C_DA's (and lower W_{HS}/W_e), the drogue parachute weight increases in order to sufficiently decelerate the vehicle at the specified deployment altitude (if a specified main chute deployment altitude is required). Shown on Fig. 17 are results for optimum suspended weight fraction (W_S/W_e) vs descent time for a two-chute system (drogue and main) for various main chute deployment altitudes, where W_S is the weight on the main chute after the heat shield and structure have been jettisoned. Sizeable descent times (5–10 min) appear to be feasible even for the lowest surface pressure model atmospheres.

The parachute system for a survivable lander would be oriented toward maximizing landed payload. Here again, a tradeoff exists between m/C_DA and W_{HS}, but now the choice of impact velocity involves an additional tradeoff with the impact attenuator weight and the weight penalties associated with ruggedizing the lander subsystems. Results of an optimization study limiting the impact loads to 1500 g's, assuming 200 fps surface winds, are shown in Fig. 18 for a range of surface pressures using a two-chute system. It is quite clear that the surface pressure has a great effect on the landed payload weight.

Landing impact attenuation system requirements

Among the methods available to the designer of an impact attenuation system are retrorockets, gas-filled bags, penetration spikes, and liquid shock absorbers and solid materials that absorb energy by yielding, fracturing, or crushing, but most attention is being directed to absorbing impact loads by means of material deformation (even systems with retrorockets usually rely on a material-deformation system for the final touchdown shock). The materials used for the latter include various foamed plastics, balsa wood, and several types of metal structures of which Al honeycomb is a commonly used example.[75] Analyses on these materials have ranged from studying the collapsing process of Al honeycomb[76] to studies of the over-all dynamics of an impact.

For fairly simple surface missions, a passive impact attenuation system is probably necessary. The design of the capsule for Rangers 3, 4, and 5 is a good example; the instrument package is completely surrounded by a sphere of balsa wood. This omnidirectional protection is especially necessary on Mars if surface winds of 200 fps are to be accounted for in the design. When a spherical design is used, it is possible to determine the so-called limiting impact velocity, which is the velocity at which the material can deliver an infinitesimal payload; that is, the deformation of the material only serves to absorb its own kinetic energy. The highest limiting impact velocity for currently available materials is ~1000 fps for balsa wood.

The payload weight penalty associated with two impact attenuation materials is indicated on Fig. 19. If the 200-fps

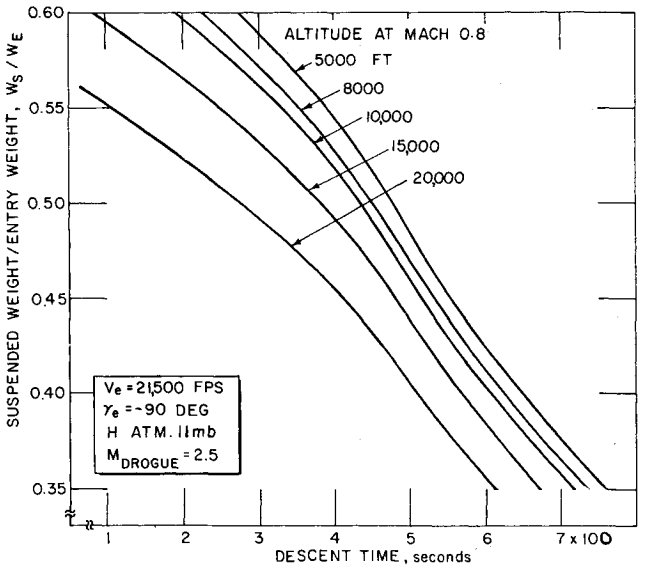

Fig. 17 Effect of descent time on suspended weight capability for different main parachute deployment altitudes. Drogue chute is deployed at Mach 2.5.

surface wind constraint is imposed, then the total impact velocity will be in the range of 210 to 250 fps, depending on the vertical descent velocity after parachute deployment. In this range of impact velocities, about half of the total landed weight consists of the impact attenuation material. Balsa wood gives a higher weight fraction than Al honeycomb, but only at the expense of higher peak deceleration levels. A further advantage of balsa wood, however, is that it is fairly transparent to radio signals, whereas Al honeycomb would have to be deployed away from the antenna after landing. If there were no surface wind, the payload for the Al honeycomb system could be increased 70%.

The possibility of impacting a small payload without a parachute has been studied[45] utilizing a balsa attenuator and configuration 5 to insure stability and high subsonic drag.

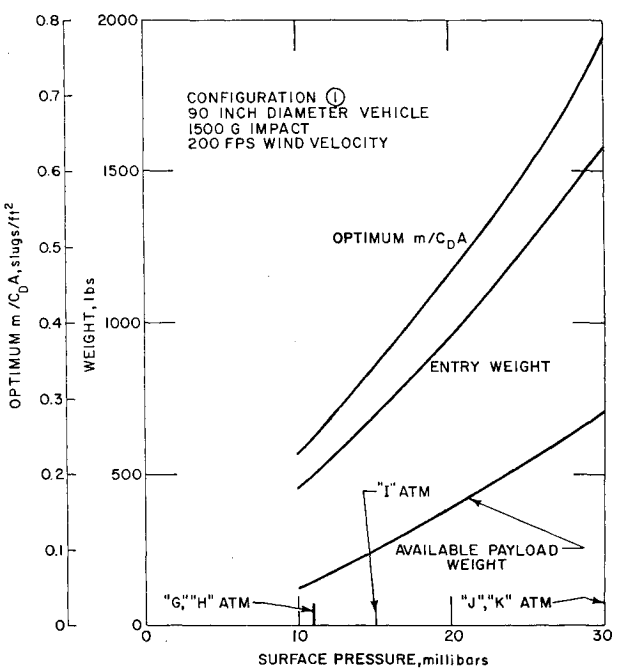

Fig. 18 Effect of atmospheric surface pressure on payload weight, entry weight, and optimum ballistic parameter for a typical short-lifetime lander.

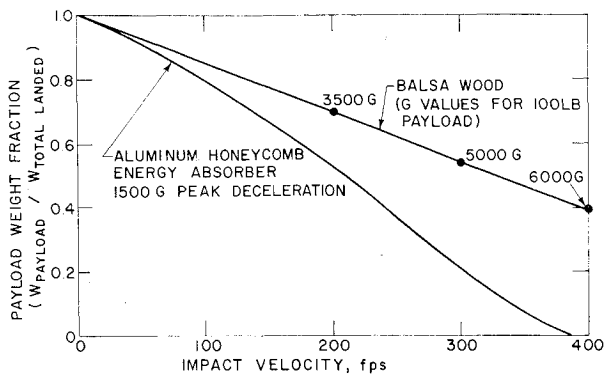

Fig. 19 Effect of landing impact velocity on payload weight fraction utilizing two different impact attenuation materials.

The feasibility of this approach is highly sensitive to the surface pressure, because m/C_DA has to be extremely low to reach low terminal velocities; hence, a large penalty in W_{HS} is incurred. On the other hand, as the m/C_DA and terminal velocity increase, the weight of impact attenuator material increases. The results of an optimization study for a 90-in. vehicle (m/C_DA of 0.15) for the 10-mb minimum pressure, yielded a landed payload of about 100 lb; the payload was found to be proportional to the surface pressure. The peak impact load is 6000 g's since the impact velocity is about 400 fps. Because of the high vertical descent velocities without a parachute, the effect of wind velocities even as high as 200 fps is still quite small.

Illustrative Mars Entry Mission Design Concepts

Atmospheric Probes

Much scientific and engineering knowledge regarding the Mars atmosphere can be gained by using a few relatively simple and lightweight instruments. Two basically different approaches are 1) a blunt, high-drag capsule that decelerates at high altitude, stores data taken during the heating and communications blackout period, and transmits it with real-time measured data during the postblackout period of descent; and 2) a dart-type, very-low-drag entry vehicle that decelerates very little during entry and can communicate continuously since it does not produce a strong, normal shock with its attendant high electron concentrations.

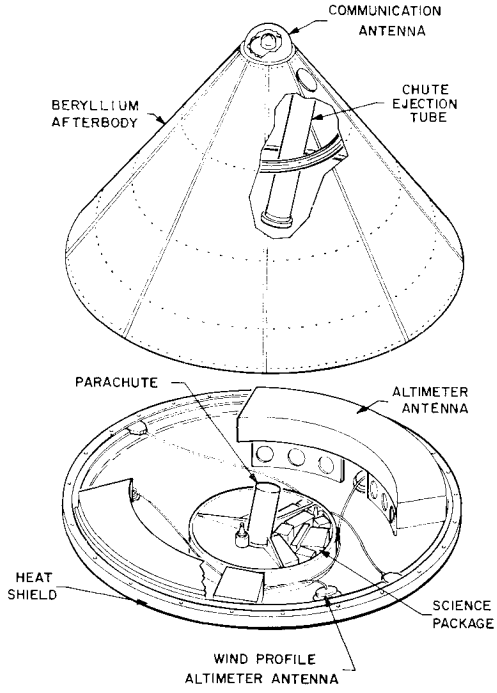

Fig. 20 Atmospheric probe design concept of utilizing parachute descent system (does not survive landing).

The deceleration history sensed by a blunt capsule can serve as a basis from which the trajectory and the atmospheric density profile can be deduced as suggested by Seiff.[53] The use of a sphere with an offset c.g. (configuration 6) has been proposed.[49, 50] The sphere concept potentially requires the least amount of accelerometer data to establish the density-altitude profile, because its C_D does not vary with α; in fact, the total resultant force on the vehicle is simply the drag. Hence, a three-axis accelerometer system and a low-bit-rate communication system transmitting only the resultant deceleration at relatively infrequent time intervals would yield adequate results. During the terminal, subsonic portion of entry, ambient pressure should be measured directly to remove ambiguities associated with the pressure predictions from the accelerometer measurements. The relatively low drag characteristics of the sphere are somewhat disadvantageous for this purpose since, to achieve subsonic terminal velocities in the low-density atmospheres, a low payload weight is required. Furthermore, the poor dynamic stability characteristics of the sphere[39] may result in large α excursions, thus necessitating omnidirectional transmitting antennas. Nevertheless, the spherical atmospheric probe can be satisfactorily designed for a weight of 25 to 40 lb and a diameter of 24 to 30 in.

Experiments that could be performed during a parachute descent are discussed by Hanel, Richtmeyer, Stampfl, and Stroud.[77] A descent time ≥ 4 min is required for accomplishing the measurements and for real-time transmission via direct link to Earth. The 4-min requirement results in the need for vehicles with $m/C_DA \simeq 0.2$ slug/ft^2 for the low-surface-pressure atmospheres. To achieve this, configurations with high C_D are desirable in order to minimize size and W_{HS}. A typical design concept for such a vehicle is shown in Fig. 20; total weight is 350 lb and the diameter is 84 in. The communication system is a 2300 Mc direct link to Earth and/or a VHF relay link to a flyby or orbiter bus. The altimeter antenna shown is a low-power (100 Mc) unit that supplements the science and wind profile measurements. Of particular interest is the experiment to determine the wind velocity profile. The parachute-suspended payload quickly acquires the average wind drift speed and three separate transmitting and receiving CW radar antennas are used to measure the total horizontal drift speed with respect to the surface. The vehicle afterbody provides assurance that the vehicle will quickly achieve stable, small-α oscillations regardless of α_r.

Slender entry vehicles, flying at $\alpha \sim 0$, can be designed so that they do not strongly shock-heat the gas, and thus the communications blackout during entry can be avoided

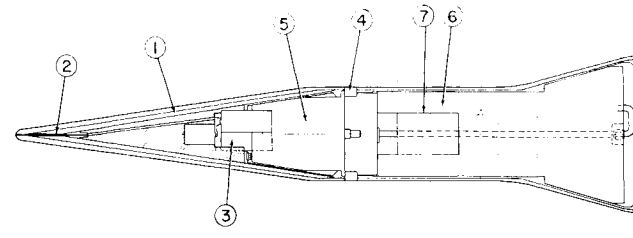

1. HEAT SHIELD (GRAPHITE)
2. PRESSURE TUBE
3. PRESSURE TRANSDUCER PACKAGES
4. ANTENNA WINDOW (QUARTZ)
5. ELECTRONICS
6. BATTERIES
7. ACCELEROMETER

Fig. 21 Slender configuration atmospheric probe design concept.

(especially for $V_e < 24{,}000$ fps).[78] A typical concept is shown in Fig. 21, which samples stagnation pressure (p_s) at relatively constant velocity. The ambient density can then be determined, since at hypersonic speeds $p_s \approx \rho_\infty V_\infty^2$. Additional static pressure ports are shown which yield a direct indication of the static pressure. Accelerometers are included in the event that a much denser atmosphere than predicted is encountered and the change in velocity becomes significant. A severe problem associated with this type of vehicle is the lack of α convergence during entry because of the very low drag of the vehicle. For example, approximate trajectory analysis indicates that the ambient pressure at peak q_∞ is $p = mg/C_DA$, so that, for $p_{surf} = 10$mb, vehicles with m/C_DA's larger than 1.6 slug/ft^2 will impact prior to peak q_∞. Consequently, unless α is controlled at entry, or stability augmentation is provided, large α oscillations could occur throughout entry with the attendant likelihood of communications blackout. This would negate the usefulness of the slender configuration.

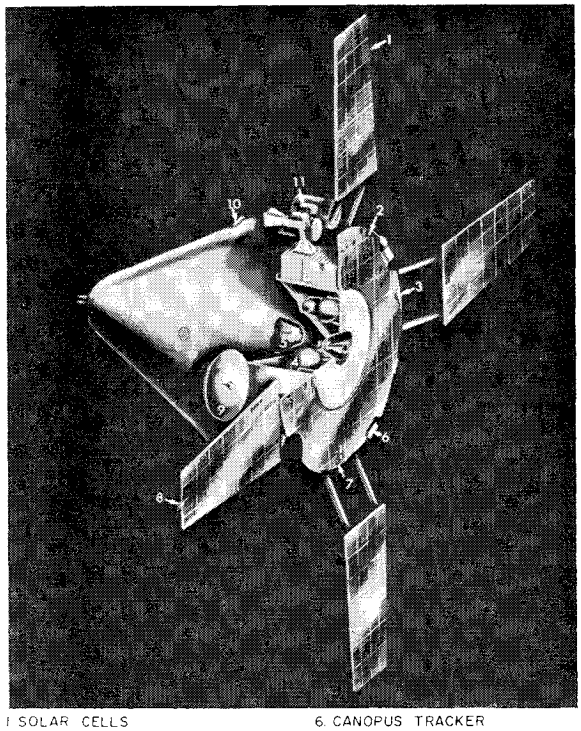

1 SOLAR CELLS
2 LIMIT CYCLE SUN SENSOR
3 ATTITUDE CONTROL JETS
4 COLD GAS TANKS
5 LANDER PROPULSION
6 CANOPUS TRACKER
7 AQUISITION SUN SENSORS
8 HEMI-OMNI ANTENNA
9 HIGH GAIN ANTENNA
10 LANDER SPIN UP ROCKETS
11 GIMBALED PAYLOAD PLATFORM

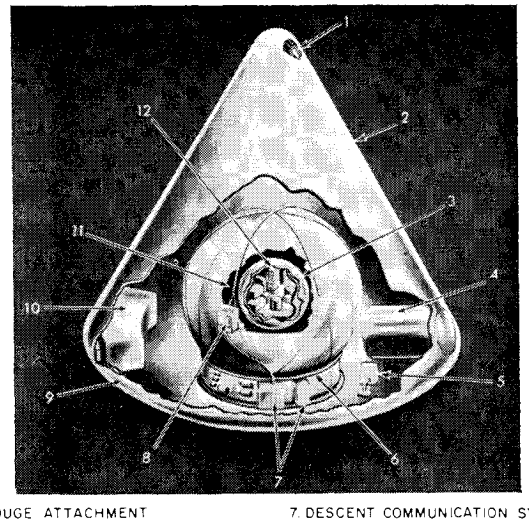

1 DROUGE ATTACHMENT
2 BERYLLIUM AFTERBODY
3 PAYLOAD FLOTATION SYSTEM
4 DROGUE CHUTE
5 PRE-ENTRY COMMUNICATING SYSTEM
6 PAYLOAD SUPPORT RING
7 DESCENT COMMUNICATION SYSTEM
8 HORN ANTENNA (S-BAND)
9 FOREBODY HEAT SHIELD SYSTEM
10 MAIN CHUTE
11 IMPACT ATTENUATION SYSTEM
12 LANDED PAYLOAD COMMUNICATION SYSTEM

64-12182

Fig. 22 Short-lifetime lander and flyby bus spacecraft concept (advanced Mariner).

Short-Lifetime (Lightweight) Landers

A lightweight lander is considered as having a short post-landing mission on the order of 6 to 12 hr. It would be transported to Mars by a flyby or orbiter bus. A lander concept, suitable for an Atlas Centaur launch, is depicted in Fig. 22. The objectives include atmospheric measurements during entry and descent, demonstration of a successful landing, and performance of a short-time biological experiment following impact. A summary of the mission constraints that lead to the choice of configuration is as follows: 1) V_e = 21,500–24,000 fps (commensurate with 1969 and 1971 launch windows); 2) γ_e (3σ limit) = 52°–90°; 3) spin stabilization during lander separation (20 rpm, followed by despin; small residual spin desirable for thermal control); 4) survive all model atmospheres (G, H, I, J, K; W_{HS} designed for worst combination); 5) drogue parachute deployment Mach No., 2.5 ± 0.5; 6) minimum deployment altitude of main chute, 8000 ft (heat shield jettisoned); 7) minimum descent time on main chute, 100 sec; 8) maximum vertical impact velocity, 60 fps; 9) wind gust velocity, 200 fps; 10) landed useful payload, 130 lb; 11) maximum loading at impact, 1500 g; and 12) maximum diameter, 100 in.

The science, communication, and power requirements for the mission together with the impact attenuation requirements lead to a 42-in.-diam spherical lander payload, which is carried within a very high-drag entry vehicle configuration, shown in Fig. 22, of 90-in.-diam. The total lander weighs 500 lb at entry, with $m/C_DA = 0.25$ slug/ft^2 and $W_{HS}/W_e = 0.21$. The heat shield and exterior shell are jettisoned after the main chute opens. The landing sequence is shown in Fig. 23.

Long-Lifetime (Heavy) Landers

The heavy lander vehicle must satisfy a number of additional mission constraints. A high-gain antenna, preferably a parabolic dish, is needed for communication directly with Earth; studies indicate that the antenna should be ~10 ft in diameter. If the winds are indeed as high as 200 fps, it will likely have to be enclosed in a radome. Further, if high winds are likely, the landing phase will probably utilize an active system to cancel out the horizontal drift velocity and also to insure a preferred direction (vertical) at impact. The entry vehicle configuration must be suitable to package and deploy the landed payload, and the attitude of the lander must be near vertical if the high-gain antenna is to deploy

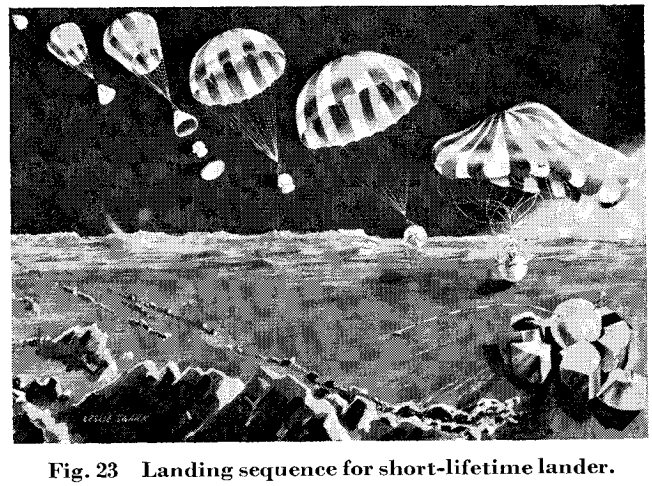

Fig. 23 Landing sequence for short-lifetime lander.

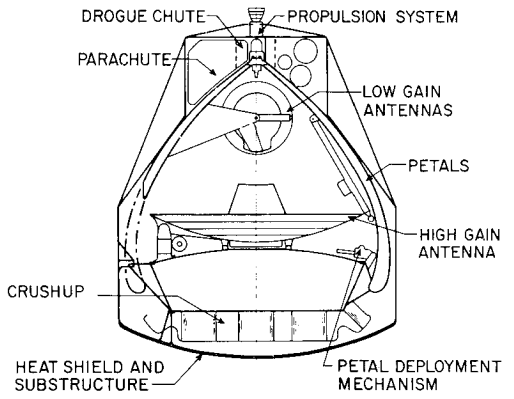

Fig. 24 Long-lifetime lander design concept for higher surface pressure atmospheric models (Shilling atmospheres).

satisfactorily. A number of scientific experiments may also require specific orientation.

A landing system concept capable of re-erecting the payload should toppling occur during landing employs a shell comprised of six petals driven by individual electric motors. By opening the petals, the science equipment is exposed directly; the petals are of *RF*-transparent material and form a protective radome for the antenna (Fig. 24) when closed. Both a high-gain and a gimbaled low-gain hemi-omni antenna are provided. The low-gain antenna is used for reception of command signals from Earth. A broad base provides impact stability and packaging room for the high gain antenna.

The launch-vehicle shroud constraints and the possibility of low surface pressures (thus requiring low m/C_DA) can restrict the total lander weight to a value well below the booster capabilities. For example, for the Saturn I-B and for an $m/C_DA = 0.25$ slug/ft^2, a maximum $W_e = 3500$ lb, which is well below the injected-weight capability of Saturn. Such limitations on W_e for a single lander have led to consideration of the use of multiple landers and/or landers with extensible drag flaps; the use of two or more landers would permit surveying more of the planet and would enhance the probability of mission success.

The particular concept of Fig. 24 was evolved to land a 1000-lb payload using the Schilling model atmospheres with surface pressures ranging from 41 to 132 mb and winds not exceeding 30 fps. The vehicle is designed to have a single stable trim point. Its high m/C_DA of 0.9 slug/ft^2 (to maximize the ratio of landed to entry weight) is appropriate for the Schilling atmospheres, but, for use in a lower-pressure model atmosphere, it needs a much lower m/C_DA of 0.28 slugs/ft^2. As the vehicle diameter must be increased by about a factor of 2 to achieve the lower m/C_DA, much more internal volume is available than is needed. Therefore, the afterbody can be made smaller, leading to a sizable reduction in the afterbody surface area and weight. In order to achieve the same landed weight, W_e must be increased substantially from 1400 to 1650 lb due to the larger W_{HS}/W_e. The parachute sizes and weights (in the event a parachute system is used) also increase significantly; the main chute diameter increases from 50 to 80 ft. The problem of packaging and integrating this much larger lander into the bus and the launch vehicle overshadows the increase in lander weight and is an important design influence of the low surface pressure atmosphere model.

Conclusions

The possibility of encountering very low atmospheric pressures and very high surface winds are the most important environmental considerations that govern the design of Mars entry and landing vehicles. In addition, long-term, reliable operation of all subsystems after undergoing sterilization and prolonged exposure to the space environment presents a difficult engineering development problem that must be emphasized for even the simplest Mars mission. Finally, all Mars mission entry vehicles are subject to space vehicle and launch vehicle integration constraints as well as other mission constraints such as trajectory, communications, and power requirements. Therefore, each mission generally requires a specific entry vehicle design, which is optimized for the particular mission objectives.

The choice of entry vehicle configuration is a compromise between the various mission constraints, the need for adequate vehicle stability, and the need for a lightweight heat shield and structure. The selection of the entry configuration should also take into account future as well as present mission requirements and should provide a growth potential to cope with changes in mission objectives and the predicted entry environment.

It is difficult to optimize the design of large-payload, long-lifetime landers until the wide range in possible atmospheric and surface conditions is narrowed through the acquisition of additional data. It is possible, however, to conservatively design lander vehicles that should survive and function even under the most unfavorable set of conditions.

References

[1] Swan, P. R. and Sagan, C., "Martian landing sites for the Voyager mission," J. Spacecraft Rockets **2**, 18–25 (1965).

[2] Lederberg, J., "Exobiology: Approaches to life beyond the earth," Science **132**, 393 (1960).

[3] Phillips, C. and Hoffman, R., "Sterilization of interplanetary vehicles," Science **132**, 991 (1960).

[4] Davies, R. and Communtzis, M., *Proceedings of the Tenth International Astronautical Congress* (Springer-Verlag, Vienna, 1960), Vol. I, p. 495.

[5] Jaffe, L., "Sterilization of unmanned planetary and lunar space vehicles—an engineering examination," Jet Propulsion Lab. TR 32-325, Pasadena, Calif., pp. 6–7 (1963).

[6] "Launch vehicle capabilities," Second NASA-Industry Program Plans Conference, News Release, NASA, Washington, D. C. (February 12, 1963).

[7] Clarke, V. C., Jr., Roth, R. Y., Scholey, W. J., and Bollman, W. E., "Design parameters for ballistic interplanetary trajectories—Part I, one-way transfers to Mars and Venus," Jet Propulsion Lab. TR 32-77, Pasadena, Calif. (January 16, 1963).

[8] Clarke, V. C., Jr., Roth, R. Y., Bollman, W. E., Hamilton, T. W., and Pfeiffer, C. G., "Earth-Mars trajectories 1964–1977," Vols. 1–7, Jet Propulsion Lab. Tech. Memo. 33-100, Pasadena, Calif. (March 15, 1964).

[9] "Systems capabilities and development schedule of the deep space instrumentation facility, 1964–68," Jet Propulsion Lab. Tech. Memo. 33-83, revision 1, Pasadena, Calif. (April 1964).

[10] Van Trees, H. L., "Optimum power division in coherent communication systems," Professional Group on Space Electronics and Telemetry pp. 1–9 (February 1963).

[11] Martin, B. D., "The Mariner planetary communication system design," Proceedings of the 1962 National Telemetering Conference, Vol. 2, Article 8-3 (May 1962).

[12] Frazier, J. P. and Page, J., "Phase-lock loop frequency acquisition study," Professional Group on Space Electronics and Telemetry., pp. 210–227 (September 1962).

[13] Viterbi, A. J., "Acquisition and tracking behavior of phase-locked loops," Jet Propulsion Lab., External Publ. 673, Pasadena, Calif. (July 1959).

[14] Develet, J. A., "A threshold criterion for phase-lock demodulation," Proc. Inst. Elec. Electron. Engrs. 349–356 (1963).

[15] Becker, H. D. and Lawton, J. G., "Theoretical comparison of binary data transmission systems," Cornell Aeronautical Lab., Inc., Rept. CA-1172-S-1 (May 1958).

[16] Shaft, P. D., "Error rate of PCM-FM using discriminator detection," Professional Group on Spece Electronics and Telemetry, pp. 131–137 (December 1963).

[17] Gupta, S. C., Transient analysis of a phase-locked loop optimized for a frequency ramp input," Professional Group on Space Electronics and Telemetry, pp. 79–84 (June 1964).

[18] Sheftelman, E., "Reducing multipath disturbances with chirp keying," Internal Publ. TIDM-F440-379, Avco RAD, Wilmington, Mass. (August 1963).

[19] Belove, L and McCarthy, R. J., "The sealed nickel-cad-

mium battery cell," Sonotone Corp., Elmsford, N. Y. (June 1963).

[20] Landau, M. B., "Fuel cell performance for Mars lander vehicle," Pratt and Whitney Aircraft, Rept. SE 120 (June 18, 1963); also Tompson, R. A., Rept. SE 133 (August 28, 1963).

[21] Van Heyst, H. P. and Cunningham, T. M., "Silicon-germanium thermoelectric power modules," 18th Annual Power Sources Conference, Atlantic City, N. J., RCA Paper St-2652 (May 1964).

[22] Harvey, R. J. and Robinson, T. C., "Evaluation of isotopic thermionic generators," Thermo Electron Corp, Waltham, Mass., 9th Annual Meeting of American Nuclear Society (1963).

[23] Koslover, M., "Status of isotopic power development," Avco RAD Tech. Release AEDM-F510-78, Report of Industry Information Meeting in Washington, D. C. (May 18–19, 1964); confidential.

[24] Kaplan, L. D., Munch, G., and Spinrad, H., "An analysis of the spectrum of Mars," Astrophys. J. **139**, 1–15 (January 1964).

[25] Rasool, S. I., "Structure of planetary atmospheres," AIAA J. **1**, 6–17 (1963).

[26] Schilling, G. F., "Limiting model atmospheres of Mars," The Rand Corp., R-402-JPL (August 1962).

[27] Grandjean, J. and Goody, R. M., "The concentration of carbon dioxide in the atmosphere of Mars," Astrophys. J. **121**, 548–552 (1955).

[28] Kuiper, G. P., *The Atmospheres of the Earth and Planets* (University of Chicago Press, Chicago, Ill., 1952), Chap. II, pp. 296–301.

[29] DeVaucouleurs, G., *Physics of the Planet Mars* (Faber and Faber Ltd., London, 1954), p. 343.

[30] Haurlan, P. N., private communication, Jet Propulsion Lab., JPL Contract 950896 (May 8, 1964).

[31] Spiegel, J. M., "Effects of Mars atmospheric uncertainties on entry vehicle design," Aerospace Eng. **21**, 63, 103–107 (December 1962).

[32] Levin, G. M., Evans, D. E., and Stevens, V., "NASA Engineering Models of the Mars Atmosphere for Entry Vehicle Design," NASA TN D-2525 (November 1964).

[33] Roberts, L., "Entry into planetary atmospheres," Astronaut. Aeronaut. **11**, 22–29 (October 1964).

[34] Shane, E. D., "Equilibrium electron density on Mars," AIAA J. **2**, 1497–1499 (1964).

[35] Levine, P., "Entry of space vehicles into planetary atmospheres Part I—Ballistic entry," Avco RAD TM-62-20, Wilmington, Mass. (April 30, 1962).

[36] Thomas, G. M. and Menard, W. A., "Experimental measurements of nonequilibrium and equilibrium radiation from planetary atmospheres," *AIAA Entry Technology Conference* (American Institute of Aeronautics and Astronautics, New York, 1964), pp. 170–185.

[37] Howe, J. T. and Viegas, J. R., "The dissociative relaxation of CO_2 behind normal shock waves," Interplanetary Missions Conference 9th Annual American Astronautical Society Meeting (January 1963).

[38] Ferri, A. and Zakkay, V., "Measurements of stagnation point heat transfer at low Reynolds numbers," J. Aerospace Sci. **29**, 847–850 (1962).

[39] Lichtenstein, J. H., Fisher, L. R., Scher, S. H., and Lawrence, G. F., "Some static, oscillatory, and free-body tests of blunt bodies at low subsonic speeds," NASA Memo. 2-22-59L (April 1959).

[40] "Study of a drag brake satellite recovery system," Vol. III, Aeronautical Systems Div. TR 61-348 (January 1962).

[41] Keyes, J. W., "Longitudinal aerodynamic characteristics of blunted cones at Mach numbers of 3.5, 4.2, and 6.0," NASA TN D-2201 (February 1964).

[42] "Mars Venus capsule parameter study," Avco RAD-TR-64-1, Vols. I and II, Contract JPL-950626, Wilmington, Mass. (1964).

[43] "Results of the second United States manned orbital space flight," NASA Sp-6 (May 1964).

[44] Dayman, B., Jr., Brayshaw, J. M., Jr., Nelson, D. A., Jafee, P., and Babineaux, T. L., "The influence of shape on aerodynamic damping of oscillatory motion during Mars atmosphere entry and measurement of pitch damping at large oscillation amplitudes," Jet Propulsion Lab. TR-32-380, Pasadena, Calif. (February 28, 1963).

[45] "Conceptual design studies of an advanced Mariner spacecraft, Vol. III, Lander design," Avco RAD-TR-64-36, Contract JPL-950896, Wilmington, Mass. (October 28, 1964).

[46] Katz, G. D. and McMullen, J. C., "Entry vehicles for unmanned planetary exploration," *AIAA Entry Technology Conference* (American Institute of Aeronautics and Astronautics, New York, 1964), pp. 1–12.

[47] Anderson, R. A., "An appraisal of structures technology," AIAA Paper 64-531 (June 29–July 2, 1964).

[48] Brown, H. K., "Spin of a parachute drag structure," Avco AERL Research Note 69 (April 1958).

[49] Seiff, A., "Developments in entry vehicle technology," AIAA Paper 64-528 (June 19–July 2, 1964).

[50] Beuf, F. G., "A simple entry system experiment for martian atmospheric measurements," AIAA Paper 64-292 (June 29–July 2, 1964).

[51] Allen, H. J., "Motion of a ballistic missile angularly misaligned with the flight path upon entering the atmosphere and its effect upon aerodynamic heating, aerodynamic loads, and miss distance," NASA TN 4048 (October 1957).

[52] Sommer, S. C. and Tobak, M., "Study of the oscillatory motion of manned vehicles entering the Earth's atmosphere," NASA Memo. 3-2-59 A (April 1959).

[53] Seiff, A., "Some possibilities for determining the characteristics of the atmospheres of Mars and Venus from gas-dynamic behavior of a probe vehicle," NASA TN D-1770 (April 1963).

[54] Jaffe, P., "Hypersonic ballistic range results of two planetary entry configurations in air and carbon dioxide/nitrogen mixtures," Jet Propulsion Lab. TR 32-543, Pasadena, Calif. (January 21, 1964).

[55] Gruszcynski, J. S. and Warren, W. P., Jr., "Experimental heat transfer studies of hypervelocity flight in planetary atmospheres," AIAA J. **2**, 1542–1550 (1964).

[56] Rose, P. H. and Stankevics, J. O., "Stagnation point heat transfer measurements in partially ionized air," AIAA J. **1**, 2752–2763 (1963).

[57] Collins, D. J., "Convective heat transfer in planetary atmospheres," Jet Propulsion Lab. TR 32-629, Pasadena, Calif. (July 1964).

[58] Hoshizaki, H., "Heat transfer in planetary atmospheres at supersatellite speeds," ARS J. **32**, 1544–1552 (October 1962).

[59] Fay, J. A. and Kemp, N. H., "Theory of stagnation point heat transfer in a partially ionized diatomic gas," AIAA J. **1**, 2471–2751 (1963).

[60] Sones, P., "Convective heating for model atmospheres of Mars," Avco RAD Tech. Memo., Wilmington, Mass. (to be published).

[61] Yos, J. M., "Transport properties of nitrogen, oxygen, hydrogen and air to 30,000°K," Avco RAD-TM-63-7, Wilmington, Mass. (March 1963).

[62] Van Tassell, W., "Convective heating in planetary atmospheres," Avco RAD-TM-63-72, Wilmington, Mass. (October 1963).

[63] Wolf, F. and Horton, T., "Effect of argon addition on shock-layer radiance of CO_2–N_2 gas mixtures," AIAA J. **2**, 1472–1474 (1964).

[64] Finson, M. L. and Kemp, N. H., "Theory of stagnation point heat transfer in ionized monatomic gases," Phys. Fluids (to be published).

[65] Rutowski, R. W. and Bushader, D., "Shock tube studies of radiative transport on an argon plasma," Phys. Fluids, **I**, 568–577 (1964).

[66] Reilly, J. P., "Stagnation point heating in ionized monatomic gases," Fluid Mechanics Lab. Publ. 64-1 (1964).

[67] James, G. S., "Experimental study of radiative transport from hot gases simulating in composition the atmospheres of Mars and Venus atmosphere," AIAA Paper 63-455 (August 1963).

[68] Fairbairn, A., "The spectrum of shock-heated gases simulating the Venus atmosphere," AIAA Paper 63-454 (August 1963).

[69] Thomas, G. M. and Menard, W. G., "Experimental measurements of nonequilibrium and equilibrium radiation from planetary atmospheres," *AIAA Entry Technology Conference* (American Institute of Aeronautics and Astronautics, New York, 1964). pp. 170–185.

[70] Adams, M. C., Georgiev, S., Levine, P., and John, R. R., "Some recent studies of new reentry problems," AIAA Preprint 63-476 (October 1963).

[71] Voyvodich, N. S. and Pope, R. B., "An investigation of the effect of gas composition on the ablation behavior of a charring material," AIAA Preprint 63-465 (August 1963).

[72] Swann, R. T., Dow, M. B., and Tompkins, S. S., "Analysis

of the effects of environment conditions on the performance of charring ablators," *AIAA Entry Technology Conference* (American Institute of Aeronautics and Astronautics, New York, 1964), pp. 259–269.

[73] Babish, C. A., III, "Hyperflo supersonic parachute," Air Force Flight Dynamics Lab., RTD Technology Briefs, Vol. I, no. 11 (November 1963).

[74] Turner, R. D., "A recovery system for a controlled descent through the martian atmosphere," Cook Electric Co.

[75] Daigle, D. L. and Lonborg, J. O., "Evaluation of certain crushable materials," Jet Propulsion Lab. TR 32-120 (January 13, 1961).

[76] McFarland, R. K., Jr., "Hexagonal cell structures under post-buckling axial load," AIAA J. **1**, 1380–1385 (1963).

[77] Hanel, R. A., Richtmeyer, L. E., Stampfl, R. A., and Stroud, W. G., "Experiments from a small probe which enters the atmosphere of Mars," NASA TN D-1899 (December 1963).

[78] Vicente, F. A., "The effects of various reentry vehicle parameters on R-F attenuation," Aerospace Corp., BSD TDR-63-227 (October 28, 1963).

MARCH-APRIL 1965 J. SPACECRAFT VOL. 2, NO. 2

Similarity Criteria for Thermal Modeling of Spacecraft

B. T. CHAO* AND G. L. WEDEKIND†
University of Illinois, Urbana, Ill.

General scaling criteria for thermal modeling of spacecraft are deduced from governing equations of the temperature field for both two- and three-dimensional cases. Surfaces are assumed to be opaque and nondiffuse; variations of bulk thermal properties with temperature are considered. Two techniques, namely, temperature preservation and material preservation, are examined in detail. Difficulties of perfect modeling are pointed out and possible compromises are suggested. For two-dimensional problems, a significant advantage may be obtained by employing models of distorted thickness. Control of apparent thermal conductivity of materials by slitting offers interesting possibilities for both steady and nonsteady simulation.

Nomenclature

Any consistent system of units may be used; the engineering system is indicated below.

a = exponent in the power function describing the dependence of thermal conductivity on temperature
A = surface area, ft²; A' = dimensionless area, A/L^2
b = exponent in the power function describing the dependence of heat capacity on temperature
c = heat capacity, Btu/ft³-°R
d = thickness, ft
E_s = solar radiation, $\int_0^\infty E_{s,\lambda}d\lambda$, Btu/hr-ft²; E_s' = dimensionless solar radiation
$E_{s,\lambda}$ = monochromatic solar radiation, Btu/hr-ft²-μ
h_J = joint conductance, Btu/hr-ft²-°R
I_λ = monochromatic intensity of radiosity, the rate at which radiant energy leaves a surface in the direction θ, ϕ, per unit solid angle, per unit wavelength, per unit surface area perpendicular to the pencil of rays, Btu/hr-ft²-μ sr; thus, for surface element dA_i, it is understood that $I_{\lambda,i} = I_{\lambda,i}(T_i, \theta_i, \phi_i)$
I = intensity of radiosity, $\int_0^\infty I_\lambda d\lambda$, Btu/hr-ft²-sr; hence I implies $I(T, \theta, \phi)$; I' = dimensionless intensity of radiosity, $I/\sigma T_0^4$
$I_{b,\lambda}$ = monochromatic intensity of radiation of a black surface, $(1/\pi)C_1\lambda^{-5}/\{[\exp(C_2/\lambda T)] - 1\}$, where $C_1 = 1.1870 \times 10^8$ Btu-μ^4/hr-ft², $C_2 = 2.5896 \times 10^4$ μ-°R
k = thermal conductivity, Btu/hr-ft-°R
L = characteristic length, ft
q_A = prescribed surface heat flux, Btu/hr-ft²
q_{net} = net rate at which radiation leaves a surface, Btu/hr-ft²; q_{net}' = dimensionless net rate at which radiation leaves a surface, $q_{net}/\sigma T_0^4$
r = distance between surface elements (see Fig. 1), ft
S = rate of internal heat generation per unit volume, Btu/hr-ft³
t = time, hr; t' = dimensionless time (Fourier number), $\bar{k}T_0^a t/\bar{c}T_0^b L^2$
T = temperature, °R; T' = dimensionless temperature, T/T_0
T_0 = characteristic temperature of the problem, °R
x, y = curvilinear orthogonal coordinates (see Fig. 1), ft; x', y' = dimensionless curvilinear orthogonal coordinates, x/L, y/L
α, γ = angles defining the direction at which incoming radiation strikes a surface coming from another surface (see Fig. 1)
β, ψ = angles defining the direction at which incoming collimated solar radiation strikes a surface (see Fig. 1)
δ, ξ = angles defining the direction at which incoming radiation strikes a surface coming from another part of the same surface (see Fig. 1)
ϵ_λ = directional monochromatic emissivity, $\epsilon_\lambda(T, \theta, \phi)$
θ, ϕ = angles defining the direction at which radiation leaves a surface (see Fig. 1)
λ = wavelength, μ
$\pi^{-1}\rho_\lambda(\alpha, \gamma)$ = monochromatic reflection function, the ratio of the rate at which monochromatic radiation is reflected from a surface in the direction θ, ϕ per unit solid angle, per unit surface area perpendicular to the pencil of rays, to the rate at which monochromatic radiation strikes a surface coming from the direction α, γ; thus, for surface element dA_i, $\pi^{-1}\rho_{\lambda,i}(\alpha, \gamma)$ implies $\pi^{-1}\rho_{\lambda,i}(T_i, \theta_i, \phi_i; \alpha_i, \gamma_i)$, and $\pi^{-1}\rho_{\lambda,i}(\delta, \xi)$ implies $\pi^{-1}\rho_{\lambda,i}(T_i, \theta_i, \phi_i; \delta_i, \xi_i)$, etc.
σ = Stefan-Boltzmann constant, 1.713×10^{-9} Btu/hr-ft²-°R⁴
ω = solid angle, sr

Received May 7, 1964; revision received October 13, 1964. The authors wish to thank J. M. F. Vickers of the Jet Propulsion Laboratory, California Institute of Technology, for his helpful suggestions during the preparation of this manuscript.

* Professor of Mechanical Engineering and Nuclear Engineering.

† Assistant in Mechanical Engineering.